Electrochimica Acta 389 (2021) 138662

Contents lists available at ScienceDirect

Electrochimica Acta

journal homepage: www.elsevier.com/locate/electacta

# Design and synthesis of novel electroactive 2,2′:5′,2″-terthiophene monomers including oxyethylene chains for solid-state flexible energy storage applications

Deniz Yiğit[a,*], Mustafa Güllü[b]

[a] Department of Basic Pharmaceutical Sciences, Faculty of Pharmacy, Lokman Hekim University, Söğütözü, Ankara 06510, Turkey
[b] Department of Chemistry, Faculty of Science, Ankara University, Beşevler, Ankara 06100, Turkey

ARTICLE INFO

*Article history:*
Received 6 January 2021
Revised 7 May 2021
Accepted 15 May 2021
Available online 25 May 2021

2,2′:5′,2″-terthiophene-based electroactive monomers
Poly(2,2′:5′,2″-terthiophene)s
Redox-active electrodes
Symmetric solid-state supercapacitors
Flexible supercapacitor devices

ABSTRACT

Here, we present the synthesis of novel poly(2,2′:5′,2″-terthiophene) derivatives containing oxyethylene pendant groups for the fabrication of high performance flexible redox-active electrode materials. The poly(3′,4′-bis(2-methoxyethoxy)-2,2′:5′,2″-terthiophene) (PSEDEN1), poly(3′,4′-bis(2-(2-methoxyethoxy)ethoxy)-2,2′:5′,2″-terthiophene) (PSEDEN2) and poly(3′,4′-bis(2-(2-(2-methoxyethoxy)ethoxy)ethoxy)-2,2′:5′,2″-terthiophene) (PSEDEN3) have been electrochemically polymerized on flexible stainless steel substrates without any binder and directly employed as redox-active materials. The effect of pendant group chain length on morphological characteristics of conducting polymer films have been systematically evaluated and correlated to the charge storage properties of redox-active electrode materials. Capacitive performance tests reveal that PSEDEN1, PSEDEN2 and PSEDEN3 could reach up to specific capacitances of 135 F $g^{-1}$, 212.8 F $g^{-1}$ and 403.3 F $g^{-1}$, respectively, at constant current density of 2.5 mA $cm^{-2}$ in the potential range of 0.4–1.8 V with good rate capability performances. In addition, symmetrical flexible solid-state supercapacitor devices based on polymer gel electrolyte have also been assembled using PSEDEN1, PSEDEN2 and PSEDEN3 coated flexible stainless steel substrates and tested by cyclic voltammetry, galvanostatic charge/discharge and electrochemical impedance spectroscopy techniques in detail. Fabricated devices (Cell 1, Cell 2 and Cell 3) have delivered maximum specific capacitances of $C_{spec}$= 29.3 F $g^{-1}$, 92.1 F $g^{-1}$ and 162.4 F $g^{-1}$, energy densities of SE= 6.35 W h $kg^{-1}$, 22.9 W h $kg^{-1}$ and 41.1 W h $kg^{-1}$ and power densities of SP= 929 W $kg^{-1}$, 937.7 W $kg^{-1}$ and 986.4 W $kg^{-1}$ at a current density of 2.5 mA $cm^{-2}$ in two-electrode cell configuration. Furthermore, flexible supercapacitor devices have achieved high cycle life performances with good capacitance retention values of 80.2%, 84.7% and 91.4% over 10 000 consecutive galvanic charge/discharge cycles at 2.5 mA $cm^{-2}$ constant current density from 0.4 to 1.8 V. Similarly, excellent mechanical stabilities have also been observed with 3.4%, 4.66% and 1.97% capacitance losses under various bending conditions from 0° to 170° for all flexible supercapacitor devices. These results confirm that PSEDEN1, PSEDEN2 and PSEDEN3 redox-active materials with gratifying capacitive performances and excellent flexibilities have a great potential for utilization in innovative flexible or wearable energy storage solutions.

Keywords



## 1. Introduction

Supercapacitors are new generation high-performance electrochemical energy storage systems that can be used in wide range from electric hybrid vehicles to portable consumer electronics. With respect to batteries, supercapacitors posses superior features such as rapid charging/discharging time, long cycle life, high charge capacity, enviromentally friendly and satisfying operational safety even though they have generally lower energy densities. Because of these more attractive properties, there has been more and more intensive interest in supercapacitor applications, recently [1–3].

Different from conventional dielectric capacitors, charge storage behavior of the supercapacitors is directly linked to features of electrode materials. When electrodes are polarized with a bias potential, opposite charges are stored at the electrode/electrolyte interface. Therefore, the physical and electrochemical features of the electrode material, such as active surface area, surface morphology and electrical conductivity, are major parameters that play a critical role in capacitive performance [4–6].

* Corresponding author.
*E-mail address:* deniz.yigit@lokmanhekim.edu.tr (D. Yiğit).

https://doi.org/10.1016/j.electacta.2021.138662
0013-4686/

Carbonaceous meterials, $\pi$-conjugated electrically conducting polymers and transition metal oxides are the most commonly used electrode materials for supercapacitor applications. Carbonaceous meterials, including CNT, CNF and graphene, store and release charges at the interface between a porous electrode material and the electrolyte through electrostatic interactions (adsorption-desorption) so-called as non-Faradaic processes. Even though carbon-based substrates are attracting considerable interest as suitable electrode materials for electrochemical energy storage applications because of their high specific surface area, highly porous morphology, better rate capability and excellent operation life, their solely physical charge-storage mechanism (electrical double-layer capacitance) leads to limited energy density and capacitive performance [5–14]. As being another class of capacitive electrode materials, metal oxides ($RuO_2$, $V_2O_5$, $MnO_2$, $TiO_2$,$SnO_2$ and NiO) [15–32] and electrically conducting polymers (ECPs) [33–35] use a Faradaic process based on fast and reversible redox reactions for charge storage as well as non-Faradaic processes. Metal oxides and ECPs, also known as redox-active pseudocapacitive materials, achieve a greater amount of charge storage and deliver higher energy denstiy than carbonaceous meterials due to the fact that a Faradaic redox process occurs not only on the surface but also in the matrix of electroactive materials. On the other hand, conducting polymer-based electroactive materials often suffer poor cycle life caused by physical degradation while many transition metal oxides have low electrical conductivity and limited electron transfer ability [35–40]. Notwithstanding the common disadvantage of poor cycle life, ECPs as redox-active pseudocapacitive materials have attracted tremendous attention for high performance supercapacitor applications in recent years owing to their higher redox capacitance, rapid Faradaic charge transfer ability, excellent flexible nature, low fabrication cost and unlimited structural modification possibilities [41–43]. Particularly, with rapid and competitive developments in the field of portable, flexible and wearable consumer electronics, many researchers have focused on desinging novel conducting polymer derivatives that can meet requirements of new generation energy storage solutions.

Polyaniline (PANI) [36,44–51], polypyyrole (PPy) [42,52–58], polythiophene (PT) [35,37,59–65] and poly(3,4-ethylenedioxythiophene) (PEDOT) [39,66–68] and their derivatives have been widely studied for both fundamental energy storage and supercapacitor device applications. These redox-active electrode materials based on PPy, PANI, PT and PEDOT have exhibited redox capacitance values between 22 and 950 F $g^{-1}$ under the different measurement conditions (2- and 3-electrode cell configuration). Recently, novel poly(3,6-dithienylcarbazole)-based conducting polymer films with high capacitive performances have been synthesized in our research group and better mechanical strength properties have been observed in micro-supercapacitor devices. The N-substituted poly(3,6-dithienylcarbazole) redox-active materials have delivered high specific capacitances ($C_{spec}$= 554–640 F $g^{-1}$). Moreover, poly(3,6-dithienylcarbazole)-based electrode materials exhibited outstanding long-term cycle life stabilities with up to 93% capacitance retention values over 10,000 charge/discharge cycles [69].

ECPs-based electrode materials are generally prepared by using two different procedures [70]. In one of these processes, a conducting polymer derivative is physically mixed with a polymeric binder and other additives, and then a slurry mixture is applied to the current collector by a typically solution-blending method. Even though this process seems like a simple method for large-scale fabrications, it leads to a considerable increase in the internal resistance of electroactive materials due to insulator polymeric binders. In the other and most common preparation method, CP films are electrochemically synthesized directly onto any substrate without using a polymeric binder. This one-step technique allows to form a homogeneous polymeric film covering the whole electrode material and to prepare thin and flexible redox-active surfaces with low internal resistance including interfacial contact resistance between the current collector and electroactive material [59,71]. The electropolymerization method also offers obtaining of different morphological structures with the same electroactive material since electropolymerization conditions such as polymerization method and type of dopant ion directly affect the morphological characteristics of the conducting polymer film [72]. In terms of storing electrical charges and reversible ion transport in the polymer matrix, the morphology is considered to be a primary parameter [73]. On the other hand, substituent changes on the polymer chain have a pronounced effect on morphology as much as the electropolymerization method. Our recent studies have shown that the altering of pendant groups on the conducting polymer backbone created remarkable differences in morphological structure of the polymeric networks. Redox-active films based on poly(terthiophene) and poly(3,6-dithienylcarbazole) containing butyl–, hexyl- and octyl- pendant groups exhibited different morphological features with increase in the alkyl chain length. Depending on the morphological structure, these polymeric electrode materials have reached a wide range of specific capacitance values (F $g^{-1}$) with an equal amount of redox-active substrate under the same conditions [74,75].

In the present study, novel conducting polymer films based on poly(terthiophene) containing oxyethylene pendant groups were synthesized by one-step electrochemically deposition method on stainless steel substrates without any binder and the effect of substituent chain length on capacitive performances of the conducting polymer films was systematically evaluated. In the light of our previous reports, it is known that it is possible to create morphological diversity for redox-active materials by changing the length of the substituents on conducting polymer structure [74,75]. With a similar approach, it was aimed to obtain different energy storage performances for poly(terthiophene)-based pseudocapacitive redox-active materials having the same $\pi$-conjugated polymer backbones, only depending on the morphological structures. Furthermore, poly(terthiophene) derivatives were electrochemically coated on stainless steel mesh current collector to create a polymeric network with highly accessible electroactive surface area. Thus, it was expected to increase dopant ion movements on redox-active matrix and enhance capacitive performance of electrode materials by creating efficient diffusion pathways or channels. Pseudocapacitive characteristics and performances of poly(3′,4′–bis(2-methoxyethoxy)–2,2′:5′,2″-terthiophene) (PSEDEN1), poly(3′,4′–bis(2-(2-methoxyethoxy) ethoxy)–2,2′:5′,2″-terthiophene) (PSEDEN2) and poly(3′,4′–bis(2-(2-(2-methoxyethoxy)ethoxy)ethoxy)–2,2′:5′,2″-terthiophene) (PSEDEN3) were evaluated by cyclic voltammetry and galvanostatic charge/discharge techniques with a standard three-electrode cell configuration. Furthermore, p-p type symmetrical flexible supercapacitor devices based on a polymer gel electrolyte were also assembled using PSEDEN1, PSEDEN2 and PSEDEN3 coated redox-active electrode materials. Two-electrode supercapacitor device performances of flexible supercapacitors were examined under various bending angles by cyclic voltammetry, galvanostatic charge/discharge and electrochemical impedance spectroscopy measurements.

## 2. Experimental

### 2.1. Materials and instrumentation

For the synthesis of 3′,4′-bis(2-methoxyethoxy)–2,2′:5′,2″-terthiophene monomers, all chemicals including 2-(tributylstannyl)thiophene, lithium perchlorate, and

tetrakis(triphenylphosphine)palladium (0) were purchased from Sigma-Aldrich and used directly without any purification. The flexible mesh stainless steel sheet (FSS) with a thickness of 0.15 mm was specially prepared with dimensions of 1 cm width and 1 cm length to be used as a current collector. Acetonitrile (ACN) was freshly prepared by fractional destillation in the presence of $P_2O_5$ before use. Lithium perchlorate ($LiClO_4$) was kept in an oven at 80 °C for 4 h before each electrochemical experiment (*Note: Drying of $LiClO_4$ is a completely safe procedure*). The silver wire ($Ag/Ag^+$) pseudo-reference electrode was calibrated using ferrocene redox couple ($Fe/Fe^+$) ($E_{1/2}$ ($Fe/Fe^+$)= 0.3 V) [76].

CEM Discover S-Class single-mode microwave instrument was used for microwave-supported synthetic procedures. $^1$H NMR and $^{13}$C NMR spectra were collected on a Varian-Mercury 400 MHz digital Fourier-transform (FT) NMR spectrometer in deuterated chloroform with TMS as an internal standard. FTIR and mass spectra were recorded with a Perkin Elmer Spectrum 100 spectrometer (crystal plate ATR apparatus) and a Waters 2695 Alliance Micromass ZQ LC/MS using a direct inlet probe, respectively. Scanning electron microscopy (SEM) images of conducting polymer films were obtained using a Zeiss Ultra Plus FE-SEM and EVO 40 500 V to 30 kV instrument. Electrochemical characterization studies and pseudocapacitive performance measurements were conducted with a Radiometer VoltaLab PST050 potentiostat/galvanostat-high voltage booster 100 V HVB100 and a Princeton Applied Research PAR-2273 potentiostat/galvanostat.

### 2.2. Synthesis of 2,2′:5′,2″-terthiophene monomers (SEDEN1, SEDEN2 and SEDEN3)

The synthesis of novel electroactive 2,2′:5′,2″-terthiophene monomers including oxyethylene chains were performed through a multi-step process. Firstly, diethyl 3,4-dihydroxythiophene-2,5-dicarboxylate was derivatized with homologous pendant groups of oxyethylene chain structure by a typical nucleophilic substitution reaction under microwave irradiation. Subsequently, 3′,4′-bis(2-methoxyethoxy)thiophene derivatives were modified for coupling reactions utilizing hydrolysis, decarboxylation and bromination reactions, respectively. 3′,4′-Bis(2-methoxyethoxy)−2,2′:5′,2″-terthiophene monomers, SEDEN1, SEDEN2 and SEDEN3, were finally obtained using the palladium-catalyzed Stille cross-coupling reactions (**Scheme 1**). The chemical structures of SEDEN1, SEDEN2 and SEDEN3 were confirmed by FTIR, $^1$H NMR, $^{13}$C NMR, mass spectroscopy and elemental analysis techniques. The synthetic procedures and spectral data of intermediates and monomers can be found in the Supporting Information.

*3′,4′-Bis(2-methoxyethoxy)−2,2′:5′,2″-terthiophene) (SEDEN1)*: Pale yellow oily product, 91%. $^1$H NMR (400 MHz, $CDCl_3$, 25 °C, TMS): $\delta$/ ppm= 3.42 (s, 6H, -$CH_3$), 3.76 (t, $J$ = 5.2 Hz, 4H, -$CH_2$-), 4.13 (t, $J$ = 4.8 Hz, 4H, -$CH_2$-), 7.0 (dd, $J$ = 7.2 Hz and $J$ = 2 Hz, 2H, Th-H), 7.23 (d, $J$ = 6.8 Hz, 2H, Th-H), 7.27 (d, $J$ = 7.8 Hz, 2H, Th-H). $^{13}$C NMR (400 MHz, $CDCl_3$, 25 °C, TMS): $\delta$/ ppm= 59.14 (-$CH_3$), 69.72 (-$CH_2$-), 70.80 (-$CH_2$-), 97.93 (Th-C5), 123.38 (Th-C7), 124.49 (Th-C9), 126.79 (Th-C8), 141.76 (Th-C6), 147.16 (Th-C4). IR (ATR) $\upsilon$/ $cm^{-1}$ 2946, 2875 (m, aliphatic C–H strecthing), 1632 (m, aromatic C=C strecthing), 1443, 1352, 1275 (m, aliphatic C–H bending), 1218, 1112 (s, -C-O- strecthing). MS (70 eV): m/z (%): 396.7 (3) [$M^+$, $C_{18}H_{20}O_4S_3$, 396.5], 337.3 (43), 279 (10), 255.1 (100), 242.4 (70), 233.3 (30), 175.1 (11), 142.9 (8). Elemental analysis: anal. calcd. for $C_{18}H_{20}O_4S_3$ (396.5): C 54.52, H 5.08; found. C 54.85, H 5.37.

*3′,4′-Bis(2-(2-methoxyethoxy)ethoxy)−2,2′:5′,2″-terthiophene) (SEDEN2):* Greenish-yellow oily product, 82%. 1H NMR (400 MHz, $CDCl_3$, 25 °C, TMS): $\delta$/ ppm= 3.36 (s, 6H, -$CH_3$), 3.54 (t, $J$ = 5.4 Hz, 4H, -$CH_2$-), 3.65 (t, $J$ = 5.6 Hz, 4H, -$CH_2$-), 3.81 (t, $J$ = 5.4 Hz, 4H,-$CH_2$-), 4.29 (t, $J$ = 4.8 Hz, 4H, -$CH_2$-), 7.0 (dd, $J$ = 7.2 Hz and $J$ = 2 Hz, 2H, Th-H), 7.22 (dd, $J$ = 6.8 Hz and $J$ = 1.2 Hz, 2H, Th-H), 7.28 (dd, $J$ = 7.8 Hz and $J$ = 3.2 Hz, 2H, Th-H). $^{13}$C NMR (400 MHz, $CDCl_3$, 25 °C, TMS): $\delta$/ ppm= 59 (-$CH_3$), 70.2 (-$CH_2$-), 70.4 (-$CH_2$-), 70.5 (-$CH_2$-), 71.9 (-$CH_2$-), 97.8 (Th-C5), 124.3 (Th-C7), 124.6 (Th-C9), 127 (Th-C8), 141.6 (Th-C6), 147 (Th-C4). IR (ATR) $\upsilon$/ $cm^{-1}$ 3095 (m, aromatic C–H strecthing), 2934, 2869 (m, aliphatic C–H strecthing), 1634 (m, aromatic C=C strecthing), 1445, 1365, 1277 (m, aliphatic C–H bending), 1200, 1110 (s, -C-O- strecthing). MS (70 eV): m/z (%): 484.4 (20) [$M^+$, $C_{22}H_{28}O_6S_3$, 484.6], 425.3 (30), 403.4 (100), 343.4 (20), 279.4 (60), 225.2 (12), 179.1 (25). Elemental analysis: anal. calcd. for $C_{22}H_{28}O_6S_3$ (484.6): C 54.52, H 5.82; found. C 54.73, H 5.44.

*3′,4′-Bis(2-(2-(2-methoxyethoxy)ethoxy)ethoxy)−2,2′:5′,2″-terthiophene) (SEDEN3):* Light brown oily product, 79%. $^1$H NMR (400 MHz, $CDCl_3$, 25 °C, TMS): $\delta$/ ppm= 3.38 (s, 6H, -CH3), 3.51 – 3,65 (m, 16H, -$CH_2$-), 3.76 (t, $J$ = 4.8 Hz, 4H, -$CH_2$-), 4.28 (t, $J$ = 4.8 Hz, 4H, -$CH_2$-), 7.01 (dd, $J$ = 7.2 Hz and $J$ = 2 Hz, 2H, Th-H), 7.22 (d, $J$ = 6.8 Hz, 2H, Th-H), 7.28 (d, $J$ = 7.8 Hz, 2H, Th-H). $^{13}$C NMR (400 MHz, $CDCl_3$, 25 °C, TMS): $\delta$/ ppm= 66.6 (-$CH_3$), 69.77 (-$CH_2$-), 70.47 (-$CH_2$-), 70.54 (-$CH_2$-), 70.57 (-$CH_2$-), 71.89 (-$CH_2$-), 117.84 (Th-C5), 123.44 (Th-C7), 124.64 (Th-C9), 126.98 (Th-C8), 134.24 (Th-C6), 144.56 (Th-C4). IR (ATR) $\upsilon$/ $cm^{-1}$ 2943, 2885 (m, aliphatic C–H strecthing), 1647 (m, aromatic C=C strecthing), 1438, 1356, 1259 (m, aliphatic C–H bending), 1223, 1118 (s, -C-O- strecthing). MS (70 eV): m/z (%): 572.3 (12) [$M^+$, $C_{26}H_{36}O_8S_3$, 572.7], 513 (18), 445.4 (5), 341.3 (12), 291.4 (14), 279.2 (17), 235.2 (18), 215 (100), 193.3 (33). Elemental analysis: anal. calcd. for $C_{26}H_{36}O_8S_3$ (572.7): C 54.52, H 6.34; found. C 54.29, H 6.67.

### 2.3. Electrochemical characterization of monomers and conducting polymer films

The electrochemical properties of 2,2′:5′,2″-terthiophene monomers were investigated by cyclic voltammetry (CV). A standard three-electrode configuration was set up in a 0.1 M $LiClO_4$/ACN supporting electrolyte system at 25 °C under a nitrogen atmosphere for CV studies. Platinum discs were used as the working electrode and counter electrode while a silver wire was employed as a Ag/Ag+ pseudo-reference electrode. The cyclic voltammograms were recorded at 150 mV $s^{-1}$ scan rate in the potential range from 0.0 to 2.0 V. Following the determination of monomer oxidation potentials, conducting polymer film-coated platinum disk electrodes were rinsed with ACN. The modified platinum disk electrodes were thereafter subjected to single scan cyclic voltammetry in monomer-free 0.1 M $LiClO_4$/ACN solution to examine redox behaviors and CV responses of conducting polymer films (PSEDEN1, PSEDEN2 and PSEDEN3). The single scan voltammograms were recorded between 0.0 and 2.0 V potential scale at 150 mV $s^{-1}$ scan rate using a standard three-electrode system. The electrochemical reversibility and stability of all conducting polymer films were evaluated by cyclic voltammetry studies performed at a scan rate of 25 mV $s^{-1}$ for 100 cycles in monomer-free 0.1 M $LiClO_4$/ACN solution.

### 2.4. Preparation and characterization of flexible redox-active electrode materials

PSEDEN1, PSEDEN2 and PSEDEN3 conducting polymer films were directly deposited on current collectors by a constant potential electrolysis technique. All constant potential electrolyses were carried out with an 3-electrode setup consisting of a flexible mesh stainless steel working electrode (FSS), a platinum counter electrode and a $Ag/Ag^+$ pseudo-reference electrode in 0.1 M

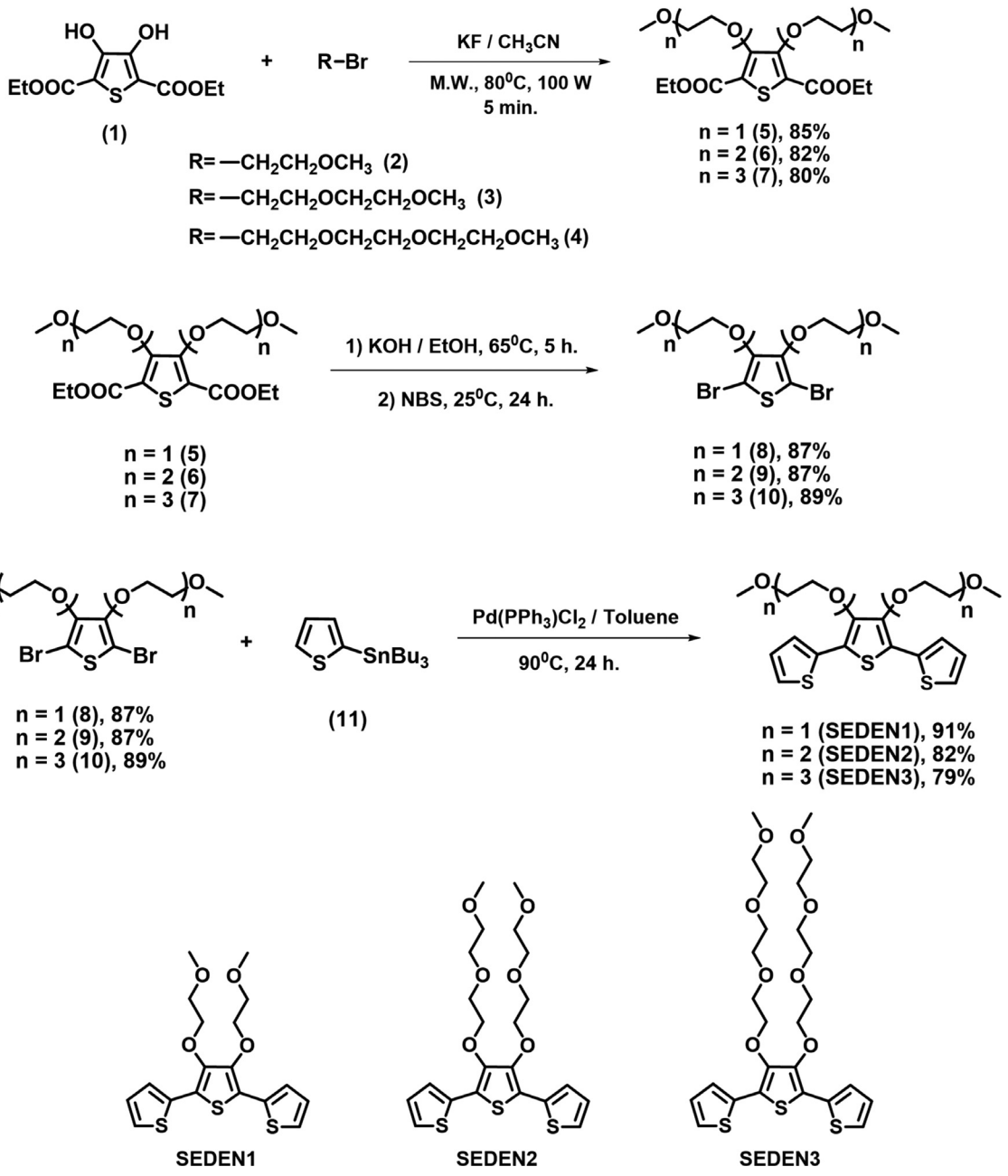


**Scheme 1.** Synthetic pathway for 2,2:5,2-terthiophene electroactive monomers, **SEDEN1, SEDEN2** and **SEDEN3**.

$LiClO_4$/ACN. PSEDEN1, PSEDEN2 and PSEDEN3-based redox-active electrode materials were prepared by applying a constant potential (1.72 V for SEDEN1, 1.80 V for SEDEN2 and 1.83 V for SEDEN3) to mesh stainless steel electrodes at 225 mC $cm^{-2}$ charge density for 115 s in the presence of 0.045 M standard monomer concentration. After each deposition, polymer coated FSS electrodes were electrochemically reduced at −0.40 V for 120 s in monomer-free supporting electrolyte solution so as to provide the electrical charge balance by expelling trapped perchlorate dopant ions on the polymer network. Afterwards, modified FSS electrodes were rinsed with ACN and they were dried at 50 °C for 2 h under vacuum atmosphere. The resulting dried polymeric mass on FSS substrates was estimated by weight with a microanalytical balance ($\Delta m = \pm$ 0.001 mg). Five parallel weightings were executed for each electrode material and the average of five weightings was accepted as the redox-active material mass for charge storage measurements. The average conducting polymer loading on modified electrode materials was measured to be 0.84 mg $cm^{-2}$ for PSEDEN1, 0.86 mg $cm^{-2}$ for PSEDEN2 and 0.87 mg $cm^{-2}$ for PSEDEN3.

The chemical structures of PSEDEN1, PSEDEN2 and PSEDEN3 redox-active films on FSS substrates were characterized by FTIR technique. The morphological properties of PSEDEN1, PSEDEN2 and PSEDEN3 conducting polymer films were also visualized by scanning electron microscopy (SEM) technique**.**

*Poly(3′,4′-bis(2-methoxyethoxy)−2,2′:5′,2″-terthiophene) (PSEDEN1)*:

IR (ATR) υ/ $cm^{-1}$ 3096 (w, aromatic C–H strecthing), 2932, 2868 (w, aliphatic C–H strecthing), 1642 (m, polyconjucated -C=C- strecthing), 1450, 1365, 1256 (m, aliphatic C–H bending), 1220, 1115 (s, -C-O- strecthing).

*Poly(3′,4′-bis(2-(2-methoxyethoxy)ethoxy)−2,2′:5′,2″-terthiophene) (SEDEN2):*

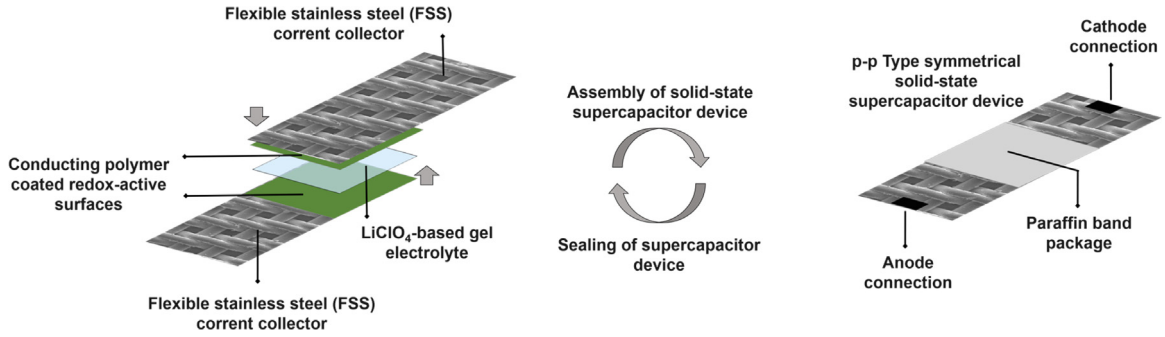


**Fig. 1.** Schematic illustration for fabrication procedure of symmetric type flexible solid-state supercapacitor devices, **Cell1, Cell2** and **Cell3**.

IR (ATR) υ/ $cm^{-1}$ 3092 (w, aromatic C–H strecthing), 2941, 2873 (w, aliphatic C–H strecthing), 1645 (m, polyconjucated -C=C- strecthing), 1441, 1382, 1270 (m, aliphatic C–H bending), 1210, 1112 (s, -C-O- strecthing).

*Poly(3′,4′-bis(2-(2-(2-methoxyethoxy)ethoxy)ethoxy)–2,2′:5′,2″-terthiophene) (SEDEN3):*

IR (ATR) υ/ $cm^{-1}$ 3089 (w, aromatic C–H strecthing), 2945, 2880 (w, aliphatic C–H strecthing), 1646 (m, polyconjucated -C=C- strecthing), 1432, 1362, 1261 (m, aliphatic C–H bending), 1221, 1116 (s, -C-O- strecthing).

### 2.5. Symmetric type flexible solid-state supercapacitor cell fabrication

The p-p type symmetric flexible solid-state supercapacitor cells were assembled in a packaged sandwich structure by using two similar redox-active electrodes separated by a gel electrolyte. The polymer gel electrolyte was prepared by a solution cast method using poly(methyl methacrylate), propylene carbonate and lithium perchlorate (Supporting Information). The warm viscous gel electrolyte was precisely spreaded to the conducting polymer coated surface of modified FSS electrodes. After that, redox-active electrodes were put together by positioning in a 180° angle to each other, ensuring the overlap active areas. The p-p type symmetric cell configuration was lightly and carefully pressed to increase the penetration of gel electrolyte layer into conducting polymer network. The solid state supercapacitor cell was wrapped several times with a paraffin band in order to seal hermetically (**Fig. 1**).

### 2.6. Capacitive performance measurements and calculations

Single electrode tests of redox-active electrodes based on PSEDEN1, PSEDEN2 and PSEDEN3 were performed with a three-electrode setup in 0.5 M $LiClO_4$/ACN electrolyte solution. In the three-electrode measurement cell, FSS substrate and silver wire were used as the counter electrode and the pseudo-reference electrode, respectively. For evaluation of the current-potential response of PSEDEN1, PSEDEN2 and PSEDEN3 redox-active electrodes, their cyclic voltammograms were recorded in the potential range 0.4 to 1.8 V using 5, 10, 25, 50, 100, 150, 250 mV $s^{-1}$ scan rates. PSEDEN1, PSEDEN2 and PSEDEN3 electrodes were then subjected to galvanostatic charge/discharge (GCD) technique over a potential window of 1.4 V at current densities of 2.5, 4.5, 6.5, 8.5, 10.5 and 12.5 mA $cm^{-2}$ to investigate the charge/discharge profile and the specific capacitance behavior.

The flexible solid-state supercapacitor cells were characterized in a two-electrode configuration following a standard charge storage performance test procedure. Different from a three-electrode setup, reference and counter electrode connections were made directly via the same redox-active electrode of the supercapacitor cell. The current-potential and charge/discharge profiles of symmetric flexible solid-state supercapacitor cells were examined by CV and GCD techniques, respectively, at bending angles of 0°, 45°, 90°, 135°, 170° The long-term cycling performances of supercapacitor devices were evaluated with a standard GCD test under at 2.5 mA $cm^{-2}$ constant current density for 10 000 charge/discharge cycles. The electrochemical impedance spectroscopy (EIS) tests were conducted in the frequency range of 10 kHz to 0.01 Hz at 0.0 V DC applied voltage using a voltage amplitude of 5 mV rms. Specific capacitance ($C_{spec}$), specific energy (SE) and specific power (SP) were calculated based on GCD curves using the following equations:

Eq. (1). $C_{spec} = (I \times t_d) / (\Delta V \times m_{ac})$

Eq. (2). $SE = [(C_{spec}) \times (\Delta V)^2] / 7.2$

Eq. (3). $SP = (3600 \times SE) / t_d$ where I, $t_d$ and $\Delta V$ describe the discharge current (mA), discharge time (s) and potential difference (V) during discharge process, respectively. $m_{ac}$ is the total mass in both electrodes for two-electrode measurements while it corresponds to the redox-active material mass in working electrodes only for three-electrode measurements.

## 3. Results and discussion

The novel 2,2′:5′,2″-terthiophene-based monomers to be used in preparation of conducting polymer films were synthesized by a multi-step method. 2,5-Dibromothiophene derivatives containing oxyethylene chain pendant groups of different lengths were prepared through microwave-assisted nucleophilic substitution reaction in the first step of the synthetic procedure. Afterwards, 2,2′:5′,2″-terthiophene-based target monomers were synthesized by palladium-catalyzed Stille cross-coupling reactions, as seen in **Scheme 1**. The monomers were fully characterized using FTIR, $^1H$ NMR, $^{13}C$ NMR, mass spectrometry and elemental analysis techniques (Supporting Information).

Following synthesis and chemical characterization studies, cyclic voltammograms of 2,2′:5′,2″-terthiophene-based monomers, SEDEN1, SEDEN2 and SEDEN3, were recorded to reveal electrochemical features of both the monomers and their conducting polymers. SEDEN1, SEDEN2 and SEDEN3 electroactive monomers exhibited typical anodic oxidation behaviors in the CV studies. In the first cycle of voltammograms, irreversible monomer oxidation peaks were observed for SEDEN1, SEDEN2 and SEDEN3 at 1.72 V, 1.80 V and 1.83 V, respectively (**Fig. 2a–c**). After the first cycle, redox waves of PSEDEN1 (1.27 V/0.90 V), PSEDEN2 (1.48 V/1.29 V) and PSEDEN3 (1.43 V/1.09 V) appeared prominetly and conducting polymer film layer began to regulary grow on the surface of platinum disk working electrodes with an increasing current density. The cyclic voltammograms clearly demonstrated that there is a slight difference between the monomer oxidation potentials of SEDEN1, SEDEN2 and SEDEN3. This small difference arises from steric hindrance effect of oxyethylene pendant groups on the monomer structures. The increase in the oxyethylene chain length of substituents at the 3ᶻ and 4ᶻ positions of terthiophene

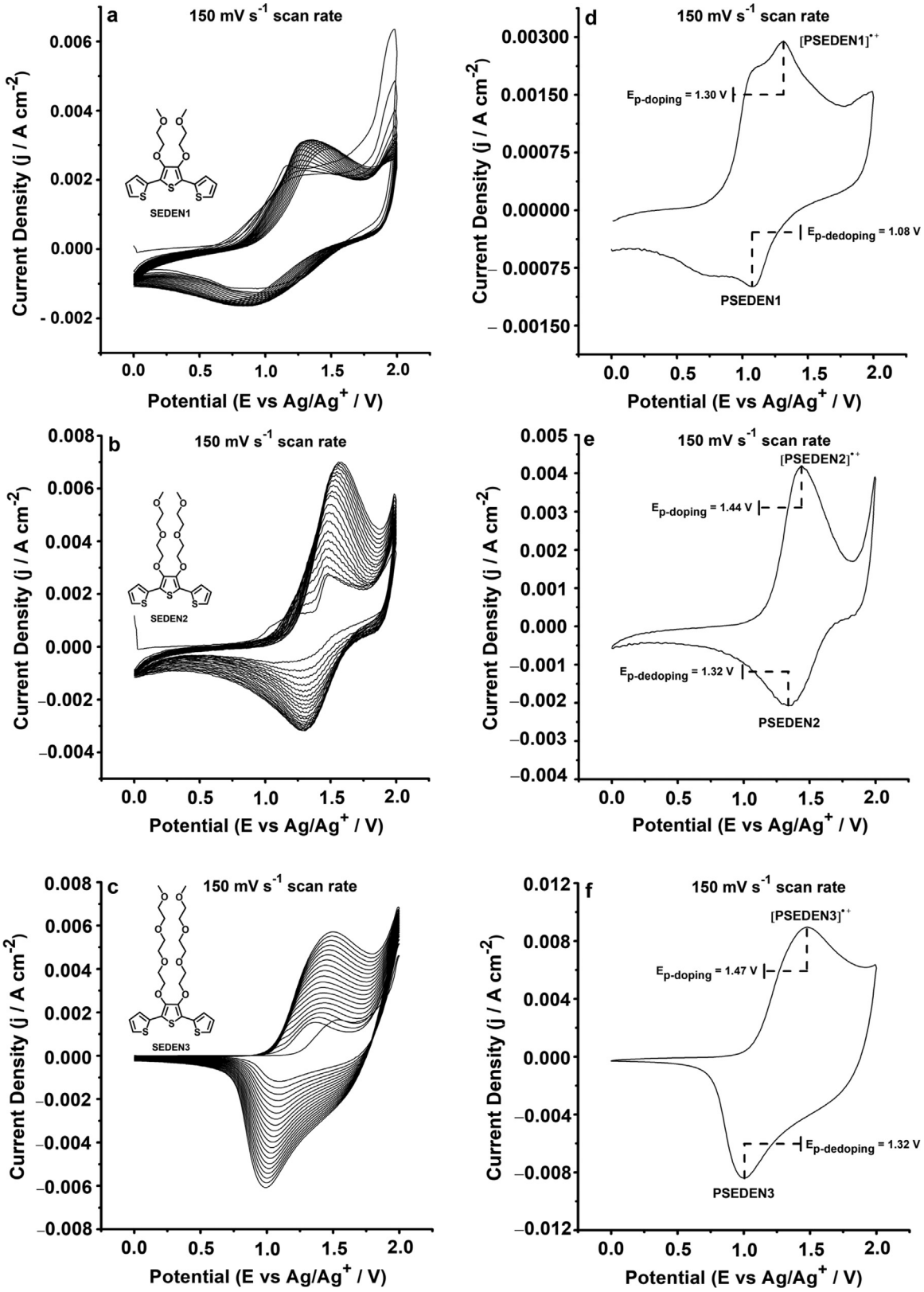


**Fig. 2.** Repetitive cyclic voltammograms for electropolymerization of (a) **SEDEN1**, (b) **SEDEN2** and (c) **SEDEN3** at scan rate of 150 mV $s^{-1}$ and single scan cyclic voltammograms in the anodic region of (d) **PSEDEN1**, (e) **PSEDEN2** and (f) **PSEDEN3** at 150 mV $s^{-1}$ scan rate in monomer-free supporting electrolyte solution.

skeleton makes steric hindrance more noticeable for electroactive monomers [77–80]. This effect partially complicates the approach of SEDEN3 to the electrode surface and the subsequent electron transfer process. Therefore, SEDEN3 was oxidized at a relatively more positive potantial compared to SEDEN1 and SEDEN2. Contrary to monomer oxidation potentials, the plots of the cathodic peak current densities versus numbers of scan reveal that SEDEN3 electroactive monomer has a higher electropolymerization rate than those of SEDEN1 and SEDEN2 (**Fig. S11** in the Supporting Information).

To examine p- and n-doping tendencies of PSEDEN1, PSEDEN2 and PSEDEN3 films, single scan voltammograms were recorded in a monomer-free solution in anodic and cathodic potential regions [81]. Reversible redox couples demonstrating p-doping characteristic were observed at 1.30 V/1.08 V for PSEDEN1, at 1.44 V/1.32 V for PSEDEN2 and at 1.47 V/1.02 V for PSEDEN3 in the anodic sweeps of current-potential curves (**Fig. 2d–f**). On the other hand, PSEDEN1, PSEDEN2 and PSEDEN3 conducting polymer derivatives did not exhibit any n-doping property in single scan voltammetry studies (**Fig. S12** in Supporting Information). The electrochemical stability of all conducting polymer films were also tested by cyclic voltammetry studies for 100 charge/discharge cycles. As can be seen in **Fig. S13**, slight differences in the voltammetry currents were observed after 100 charge/discharge cycles, indicating high electrochemical stability and reversibility characteristics for PSEDEN1, PSEDEN2 and PSEDEN3 polymeric materials.

In the light of results obtained from cyclic voltammetry studies, SEDEN1, SEDEN2 and SEDEN3 electroactive monomers were electrochemically polymerized on flexible mesh stainless steel working electrodes (FSS). Constant potential electrolysis method was especially preferred in the preparation of PSEDEN1, PSEDEN2 and PSEDEN3 coated electrode materials in order to better control the mass loading on FSS current collector substrates and to provide a more homogeneous redox-active layer. Thanks to constant potential electrolyses performed at suitable monomer oxidation potentials, similar amounts of the polymeric electroactive material were loaded per FSS current collectors, which will ensure that performance comparison among PSEDEN1, PSEDEN2 and PSEDEN3-based redox-active electrode materials. In the FTIR spectra of PSEDEN1, PSEDEN2 and PSEDEN3, the strong absorption bands at around 1640 $cm^{-1}$ which is originated from polyconjugation prove that all electroactive monomers have been successfully polymerized on the FSS substrates. In addition to FTIR spectra, the morphological properties and diversity of PSEDEN1, PSEDEN2 and PSEDEN3 polymeric networks were also examined by SEM observations. The top-view SEM images at different magnifications in **Fig. 3a–i** endorse the formation of conducting polymer layers across each FSS current collector substrate surface. On the other hand, it can be clearly seen from **Fig. 3** that the PSEDEN3 film grew more regularly on FSS substrate than PSEDEN1 and PSEDEN2 layers. This obvious variation in morphological properties is due to the difference in length of pendant oxyethylene chains on poly(terthiophene)-based polymer backbones, as envisaged. Prolongation of oxyethylene chains as pendant groups on the structure of SEDEN1, SEDEN2 and SEDEN3 monomers causes an apparent physical phenomenon for electroactive monomers and their oligomers or polymers. The increase in the length of oxyethylene side chains decreases substituent mobility at the 3≠ and 4≠positions of terthiophene monomers owing to the intense polar interactions between oxyethylene chains [82–86]. This effect originating from solubility and hydrophobicity in acetonitrile-based electrolytic media allows the formation of more uniform polymeric layers on FSS substrates during the electropolymerization process since relatively lower mobility of substituents provides the growth of oligomer/polymer chains in a certain direction [74,75]. Hence, PSEDEN3 exhibited a more regular and homogeneous surface distribution on the current collector than those of PSEDEN1 and PSEDEN2. Furthermore, as can be understood from **Fig. 3a–i**, PSEDEN3 possess more suitable polymeric networks for reversible ion movements in charge and discharge cycles.

This morphological advantage of PSEDEN3-based redox-active electrode material will likely enhance its charge storage capacity by means of more and effective ion diffusion pathways in the structure of a three-dimensional network, as expected. Conversely, irregular and agglomerated morphological behaviors were observed for PSEDEN1 and PSEDEN2 in SEM images, which can be attributed to the self-aggregation caused by the low solubility properties of the shorter oxyethylene chain pendant groups (methoxyethoxy- and 2-[2-*methoxyethoxy*]ethoxy- chains). The irregular polymeric networks of PSEDEN1 and PSEDEN2 are likely to create a barrier against ion diffusion and penetration in the three-dimensional structures. These theoretical predictions were supported by the plots of log [peak current] versus log [scan rate] prepared for the conducting polymer films (**Fig. S14** in the Supporting Information). The corresponding slopes for PSEDEN1 ($m \approx 0.71$) and PSEDEN2 ($m \approx 0.68$) redox-active materials indicate limited ion mobility during charge/discharge processes in PSEDEN1- and PSEDEN2-based polymeric networks compared to the matrix of PSEDEN3 ($m \approx 0.60$). As a result, SEM images recorded for PSEDEN1, PSEDEN2 and PSEDEN3-based redox-active electrodes clearly reveal that the prolongation of oxyethylene pendant groups in conducting polymer chains affecting the remarkable variety of morphologies of conducting polymer films, as intended.

Before comprehensive capacitive performance evaluations, all redox-active materials were subjected to CV in potential ranges between 0.0 and 2.0 V at a constant scan rate of 150 mV $s^{-1}$ to identify their ideal working potential scale. In the CV studies, the most ideal current-potential (I-V) profiles close to rectangular-like shape were observed in the potential window of 0.4–1.8 V for all ECP-based electrode materials. Hence, the potential scale of 0.4–1.8 V was determined as optimal operating potential range for all electrochemical capacitive performance measurements (**Fig. S15** in the Suppoting Information).

The pseudocapacitive behaviors of PSEDEN1, PSEDEN2 and PSEDEN3-based electrode materials were evaluated with CV and GCD techniques. To examine current-potential responses and charge/discharge characteristics of the respective ECP electrodes, cyclic voltammograms were initially recorded between 0.4–1.8 V at various scan rates ranging from 5 to 250 mV $s^{-1}$. The I-V curve of non-Faradaic capacitive materials is a rectangular-like and mirror-image shape which is defined as ideal double-layer capacitive behavior [14]. However, deviations from ideal rectangular-like profile are generally observed for pseudocapacitive materials such as conducting polymers due to their intensive Faradaic redox reactions during charge/discharge processes as well as non-Faradaic double-layer characteristic [33]. As can be seen in **Fig. 4a–c**, PSEDEN1, PSEDEN2 and PSEDEN3-based electrode materials exhibited shuttle-like I-V profiles, as an expected response from redox-active capacitive materials. The efficiency of charge/discharge of redox-active pseudocapacitive materials generally decreases as scan rate is gradually increased because of relatively lower ion diffusion rate in the conducting polymer film network at high rates. This distorts the symmetries of the I-V curves and causes shape deformations in CV profiles for long-term cycles. **Fig. 4a–c** obviously reveal that PSEDEN1, PSEDEN2 and PSEDEN3-based redox-active electrode materials maintained their initial CV shapes at even high scan rates (250 mV $s^{-1}$). These responses mean that PSEDEN1, PSEDEN2 and PSEDEN3 electrodes possess fast and highly reversible redox capability characteristics as a result of their sufficiently fast ion transportion abilities during Faradaic charge/discharge proceses [87,88]. On the other hand, PSEDEN3-based redox-active material exhibited both larger CV area

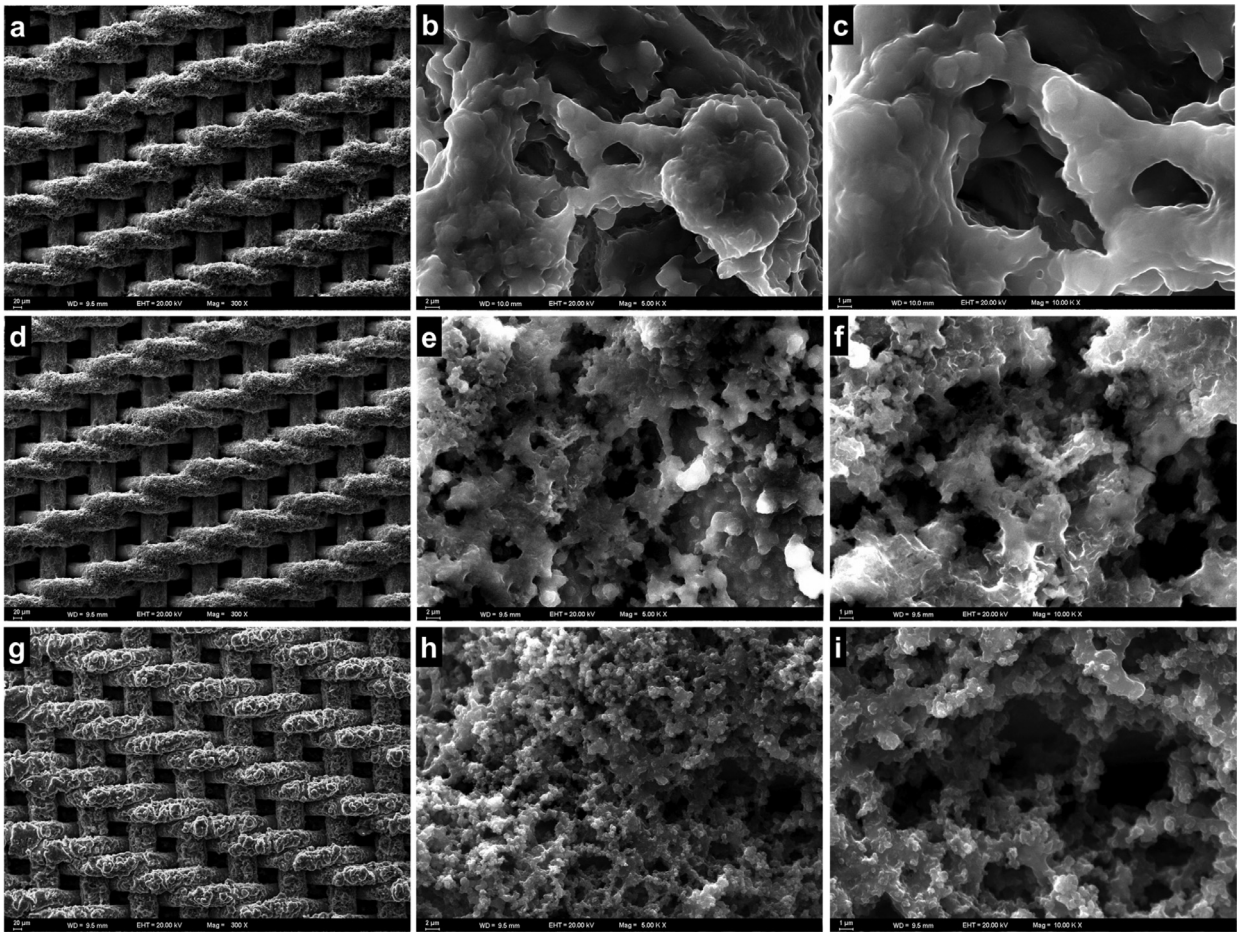


**Fig. 3.** Top-view SEM images with different magnifications of (a–c) **PSEDEN1**, (d–f) **PSEDEN2** and (g–i) **PSEDEN3**-based polymeric redox-active layers on FSS substrate.

and higher current density than those of PSEDEN1 and PSEDEN2 under the same conditions. Preliminary results obtained from CV studies confirm that PSEDEN3 polymeric films have better pseudocapacitive behavior and charge storage performance compared to PSEDEN1 and PSEDEN2.

The charge storage properties and performances of PSEDEN1, PSEDEN2 and PSEDEN3 redox-active electrodes were investigated in more detail by GCD technique. As presented in **Fig. 5a–c**, all redox-active electrode materials demonstrated nearly triangular charge/discharge profiles with very small ohmic drop values (IR-drop= 0.07 V for PSEDEN1, 0.05 V for PSEDEN2 and 0.04 V for PSEDEN3) at 2.5 mA $cm^{-2}$ constant current density over an optimum operating potential window of 1.4 V (0.4–1.8 V).

The symmetrical GCD curves mean excellent balanced and highly reversible Faradaic charge and discharge property for PSEDEN1, PSEDEN2 and PSEDEN3 redox materials, pointing to an ideal GCD characteristic. On the other side, negligible ohmic drop values reveal that PSEDEN1, PSEDEN2 and PSEDEN3-based electrodes have low internal resistances. The single electrode specific capacitance ($C_{spec}$) values for PSEDEN1, PSEDEN2 and PSEDEN3 were also calculated utilizing GCD curves in accordance with Eq. (1). The results of charge storage capacity measurements show that the PSEDEN3-based redox active material (403.3 F $g^{-1}$) delivered a significantly higher gravimetric capacitance than those of PSEDEN2 (212.8 F $g^{-1}$) and PSEDEN1 (135 F $g^{-1}$) at a constant current density of 2.5 mA $cm^{-2}$. Superior charge storage capacity of the PSEDEN3 electrode can be directly associated with its morphological structure. As discussed earlier, it can be said that PSEDEN1 and PSEDEN2 redox-active materials were able to store a limited number of ions since their agglomerated structures created a barrier effect for ion diffusions or mobilities in electroactive polymeric network. GCD measurements indicate that PSEDEN1, PSEDEN2 and PSEDEN3 are promising redox-active electrodes for practical supercapacitor applications in terms of competing with many poly(thiophene)-based pseudocapacitive materials previously reported in the literature [34,63,74,89–91] (**Table 1**). These results also reveal that different charge storage capacities could be obtained with conducting polymer derivatives having similar chemical structures only depending on the pendant group diversity (different alkyl- and oxyethylene- chains) [74].

To enlighten rate capabilities of PSEDEN1, PSEDEN2 and PSEDEN3-based redox-active electrode materials, GCD studies were repeated for different current densities (from 4.5 mA $cm^{-2}$ to 12.5 mA $cm^{-2}$) over the potential range of 0.4 to 1.8 V. The specific capacitance value of many pseudocapacitive materials decreases considerably depending on the increase in current density owing to restricted ion duffision at high current densities. Also, a limited ion diffusion rate causes an increase in IR-drop value and distortion of symmetry in GCD curves. As is apparent from **Fig. 5a–c**, PSEDEN1, PSEDEN2 and PSEDEN3 pseudocapacitive materials exhibited capacitance retention performances of 56.7% (from 135 F $g^{-1}$ to 76.6 F $g^{-1}$), 72.6% (from 212.8 F $g^{-1}$ to 154.5 F $g^{-1}$) and 69.3% (from 403.3 F $g^{-1}$ to 279.5 F $g^{-1}$), respectively, not with standing a five-fold increase in current density. Furthermore, PSEDEN1, PSEDEN2 and PSEDEN3-based electrodes maintained initial GCD shapes even at high current density values (**Fig. 5e**). These charge/discharge behaviors as a function of increasing current density endorse that all polymeric redox-active materials have satis-

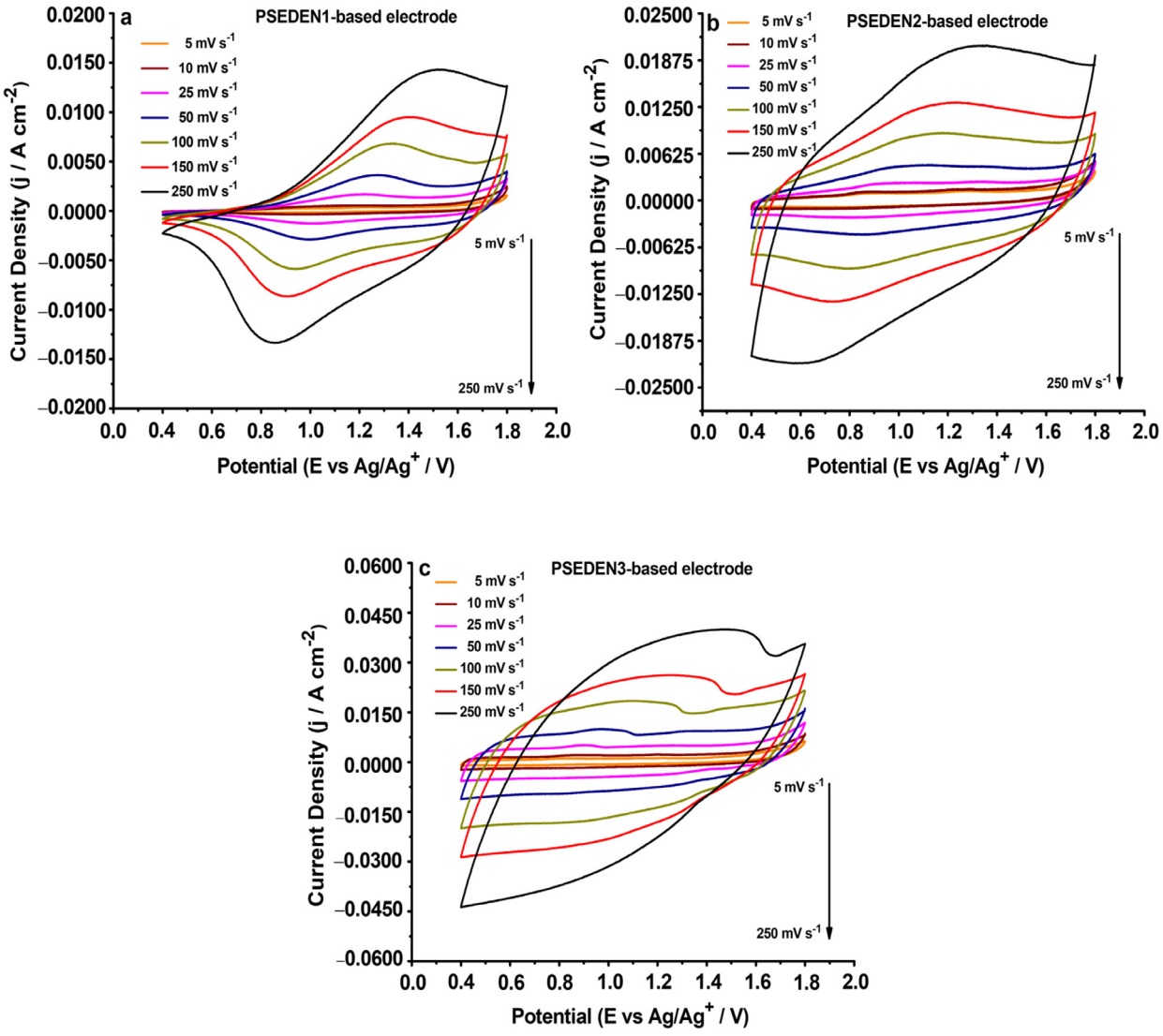


**Fig. 4.** Current-potential profiles (a) **PSEDEN1**, (b) **PSEDEN2** and (c) **PSEDEN3** polymeric flexible redox-active electrodes materials at various scan rates (from 5 to 250 mV $s^{-1}$) in 3-electrode cell configuration.

factory charge/discharge rate capabilities resulting from fast charge transfer features. The high rate capability property is an important performance indicator showing that the pseudocapacitive electrode material has the potential to be used in high power energy stroage applications.

In addition to single electrode performance evaluations, the capacitive performances of p-p type symmetric flexible supercapacitor device assembled by using the three redox-active electrode materials were also examined in a typically two-electrode cell system [92]. Unlike a three-electrode setup, potential applied to the supercapacitor system is almost equally shared by both anode and cathode materials in a two-electrode measurement technique. This offers the possibility to calculate charge storage capacity, energy and power density for the whole supercapacitor device rather than only the working electrode. Accordingly, the two-electrode cell configuration allows to obtain more meaningful and realistic results for capacitive performance evaluation. Moreover, electrochemical data acquired by two-electrode measurements provide valuable insights about the employment of redox-active electrode materials in actual supercapacitor applications. p-p type flexible supercapacitor devices Cell 1 (PSEDEN1), Cell 2 (PSEDEN2) and Cell 3 (PSEDEN3) were initially subjected to CV in order to make a qualitative comparison of capacitive performances. As can be seen in Fig. 6**a–c**, Cell 3 not only gives a I-V profile closer to rectangular shape than those of Cell 1 and Cell 2 but also a remarkably larger normalized CV area in the 0.4–1.8 V potential range. These CV responses mean a better pseudocapacitive behavior for Cell 3 compared to Cell 1 and Cell 2 and are in alignment with results obtained from three-electrode configuration measurements. The reflection of fast and highly reversible redox charge/discharge characteristics of PSEDEN1, PSEDEN2 and PSEDEN3 redox-active materials on the flexible device performances is clearly observed in the CV curves of Cell 1, Cell 2 and Cell 3. No evident distortion was found in the rectangular-like I-V profile of Cell 3 and quasi-rectangular CV shapes of Cell 1 and Cell 2 with an increasing scan rate, indicating fast ion transportion ability in the flexible supercapacitor devices based on polymer gel electrolyte (Fig. 6**a–c**).

Solid-state, flexibility and mechanical stretching properties of Cell 1, Cell 2 and Cell 3 were also tested by means of CV studies at a 250 mV $s^{-1}$ scan rate for the different bending angles (0, 45, 90, 135 and 170°). The cyclic voltammograms in Fig. 6**d–f**. depict that Cell 1, Cell 2 and Cell 3 could maintain their CV loop shapes with bending angles from 0° to 170° Moreover, almost no change in normalized CV areas was observed for Cell 1, Cell 2 and Cell 3

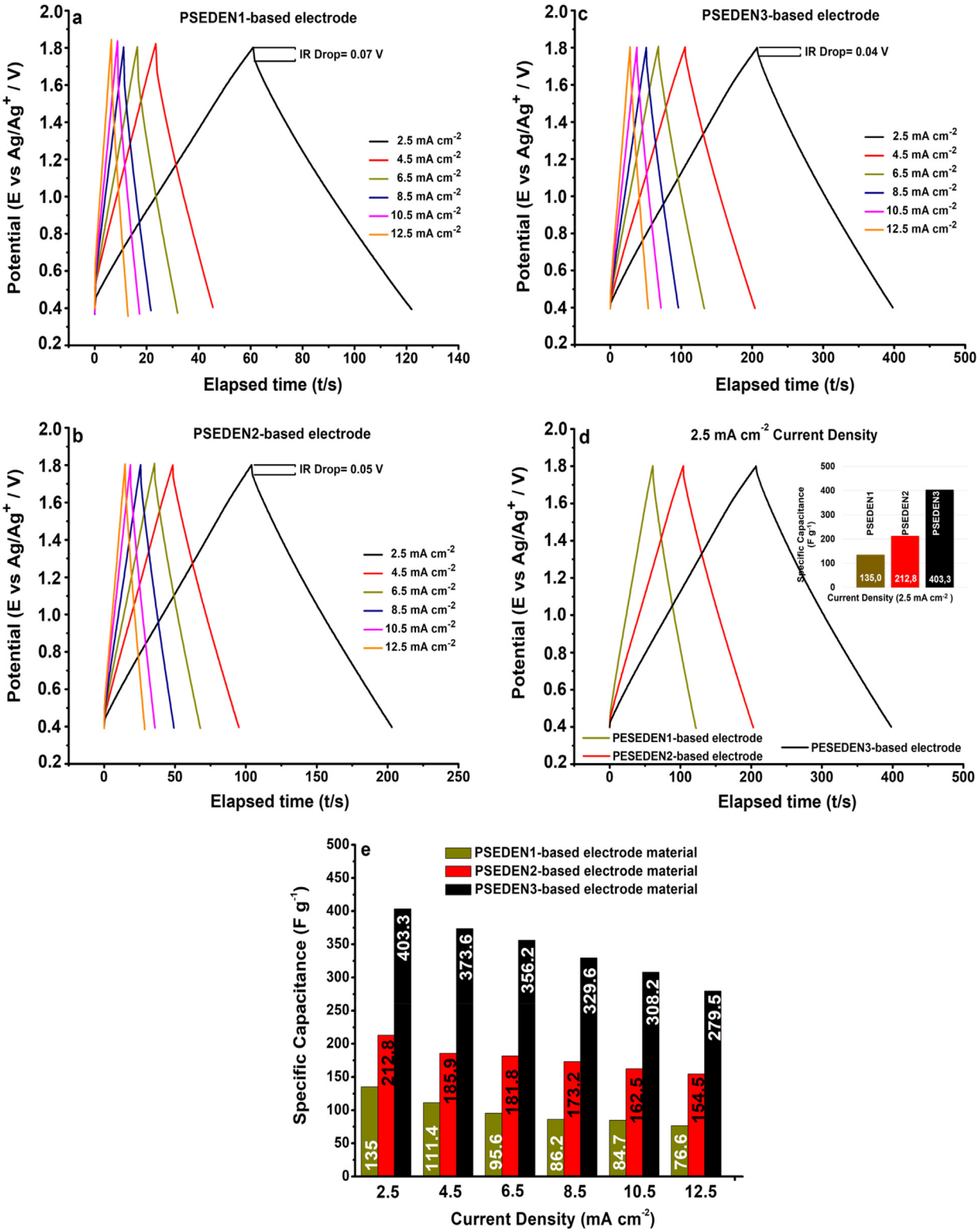


**Fig. 5.** GCD curves of (a) **PSEDEN1**, (b) **PSEDEN2** and (c) **PSEDEN3** polymeric flexible redox-active electrodes materials at different current densities from 2.5 to 12.5 mA $cm^{-2}$, (d) comparative GCD plots of electrode materials at 2.5 mA $cm^{-2}$ current density and (e) specific capacitance changes of **PSEDEN1, PSEDEN2** and **PSEDEN3** as a function of current density.

even at extreme bending condition (170°). The above results reveal that our p-p type symmetric flexible solid-state supercapacitor devices possess admirable flexibility, mechanical stretching and solidity features.

Fig. 7**a–c** shows that the galvanic cycling profiles plotted for Cell 1, Cell 2 and Cell 3 are all similar to trends observed in three-electrode measurements. Typical triangular charge/discharge curves with small ohmic drop values (IR-drop= 0.15 V for Cell 1,

**Table 1**
Charge storage performances of polythiophene-based different redox-active materials.

| Polymeric redox-active material | Operating potential range | Supporting electrolyte | Specific capacitance ($C_{spec}$) | Ref. |
|---|---|---|---|---|
|  | −0.60 – 0.80 V | 0.1 M $Na_2SO_4$ | 103 F $g^{-1}$ at 0.3 A $g^{-1}$ | [89] |
|  | 1.15 – 2.00V | 1 M $Et_4NBF_4$ / PC | 190 F $g^{-1}$ at 0.3 A $g^{-1}$ | [63] |
|  | −0.50 – 0.90 V | 0.1 M $NaClO_4$ | 176 F $g^{-1}$ at 0.75 mA $cm^{-2}$ | [90] |
| 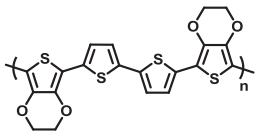 | 0.0 – 1.00 V | 0.1 M $Bu_4NPF_6$ / MeCN | 171 F $g^{-1}$ at 1 A $g^{-1}$ | [91] |
| 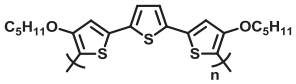 | −0.27 – 1.03 V | 1 M $Et_4NBF_4$ / PC | 190 F $g^{-1}$ | [34] |
| 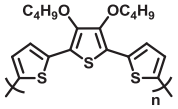 | 0.0 – 1.60 V | 0.5 M $Bu_4NBF_4$ / MeCN | 94.3 F $g^{-1}$ at 2.5 mA $cm^{-2}$ | [74] |
| 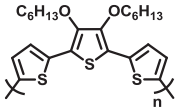 | 0.0 – 1.60 V | 0.5 M $Bu_4NBF_4$ / MeCN | 227.3 F $g^{-1}$ at 2.5 mA $cm^{-2}$ | [74] |
| 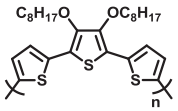 | 0.0 – 1.60 V | 0.5 M $Bu_4NBF_4$ / MeCN | 443 F $g^{-1}$ at 2.5 mA $cm^{-2}$ | [74] |
| 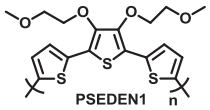 | 0.4 – 1.80 V | 0.5 M $LiClO_4$ / MeCN | 135 F $g^{-1}$ at 2.5 mA $cm^{-2}$ | This work |
| 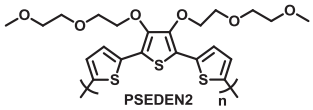 | 0.4 – 1.80 V | 0.5 M $LiClO_4$ / MeCN | 212.8 F $g^{-1}$ at 2.5 mA $cm^{-2}$ | This work |
| 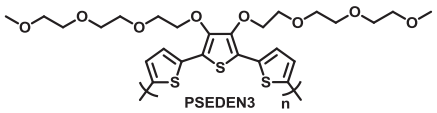 | 0.4 – 1.80 V | 0.5 M $LiClO_4$ / MeCN | 403.3 F $g^{-1}$ at 2.5 mA $cm^{-2}$ | This work |

0.06 V for Cell 2 and 0.06 V for Cell 3) were observed for each symmetric flexible solid-state supercapacitor devices at 2.5 mA $cm^{-2}$ constant current density in the potential range of 0.4 and 1.8 V. GCD shapes of Cell 1, Cell 2 and Cell 3 reveal that PSEDEN1, PSEDEN2 and PSEDEN3 electrode materials exhibited highly reversible charge and discharge characteristics during charging and discharging steps in polymeric gel electrolyte medium just as in the liquid supporting electrolyte media. As illustrated in **Fig. 7d**, Cell 3 shows considerably longer charge and discharge duration than those of Cell 1 and Cell 2, meaning that Cell 3 stored relatively more electrical charges.

This more superior capacitive performance of Cell 3 can be directly attributed to the appropriate morphological structure of PSEDEN3-based redox-active electrode material, as expected. On the other hand, a quantitative assesment of the capacitive performances was made by calculating specific capacitance ($C_{spec}$, F $g^{-1}$), energy density (SE, Wh $kg^{-1}$) and power density (SP, W $kg^{-1}$) values based on the GCD curves at 2.5 mA $cm^{-2}$ constant current density for all symmetric flexible solid-state supercapacitor devices and listed in **Table 2**.

The suitable three-dimensional network, more porous structure and relatively lower ohmic drop value of PSEDEN3-based material was believed to result in better electrochemical capacitive performance and longer discharging duration for Cell 3 compared with Cell 1 (PSEDEN1) and Cell 2 (PSEDEN2). As seen from **Table 2**, Cell 3 reached 162.4 F $g^{-1}$ specific capacitance, which was approximatly 5.5 and 1.7 times higher than those of Cell 1 (29.3 F $g^{-1}$) and Cell 2 (92.1 F $g^{-1}$). In addition to their charge storage capacities, Cell 1, Cell 2 and Cell 3 also delivered maximum energy densities of 6.35 W h $kg^{-1}$, 22.9 W h $kg^{-1}$ and 41.1 W h $kg^{-1}$, respectively. On the other hand, satisfactory gravimetric power density values as high as 929, 937.7 and 986.4 W $kg^{-1}$ were obtained for Cell 1, Cell2 and Cell 3 in galvanic charge/discharge performance tests. To determine the change in gravimetric capacitance during galvanostatic cycling, the charge storage performances of flexible solid-state supercapacitor devices were tested at a current density of 4.5, 6.5, 8.5, 10.5 and 12.5 mA $cm^{-2}$ over the potential range of 0.4–1.8 V. When the current density was gradually increased to five times, 48.2%, 31.1% and 33% falls in specific capacitance were observed for Cell 1 (from 29.3 to 15.2 F $g^{-1}$), Cell 2 (from 92.1 to 63.5 F $g^{-1}$) and

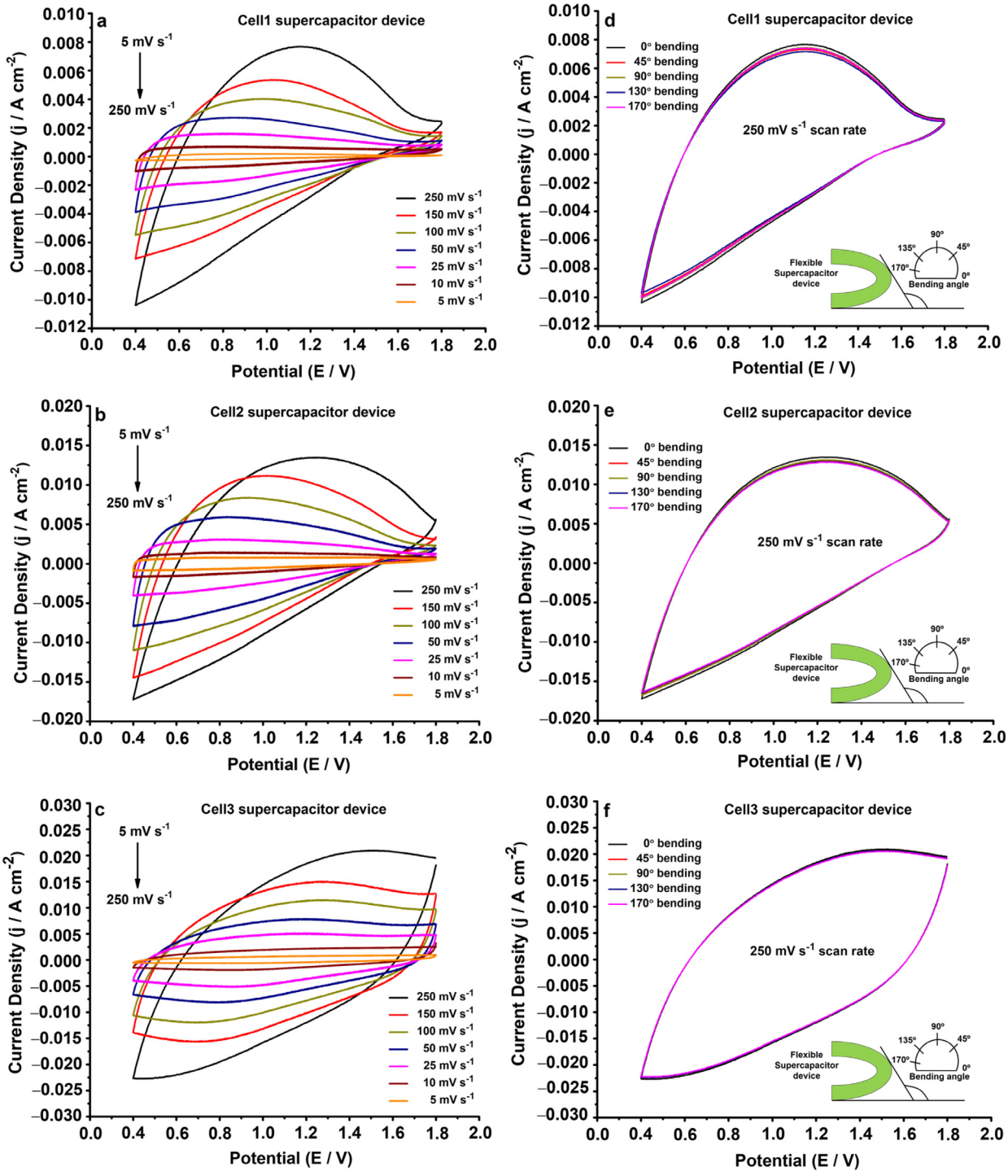


**Fig. 6.** Cyclic voltammograms of (a) **Cell1**, (b) **Cell2**, (c) **Cell3** solid-state flexible supercapacitor devices at various scan rates (from 5 to 250 mV $s^{-1}$) in 2-electrode cell configuration and current-potential profiles of (d) **Cell1**, (e) **Cell2** and (f) **Cell3** at 250 mV $s^{-1}$ scan rate under different bending conditions.

**Table 2**
Capacitive performance parameters of flexible solid-state supercapacitor devices (Cell1, Cell2 and Cell3).

| Flexible solid-state supercapacitor device configuration | | | |
|---|---|---|---|
| | Cell 1 | Cell 2 | Cell 3 |
| Specific Capacitance ($C_{spec}$) | 29.3 F $g^{-1}$ | 92.1 F $g^{-1}$ | 162.4 F $g^{-1}$ |
| Energy Density (SE) | 6.35 W h $kg^{-1}$ | 22.9 W h $kg^{-1}$ | 41.1 W h $kg^{-1}$ |
| Power Density (SP) | 929 W $kg^{-1}$ | 937.7 W $kg^{-1}$ | 986.4 W $kg^{-1}$ |

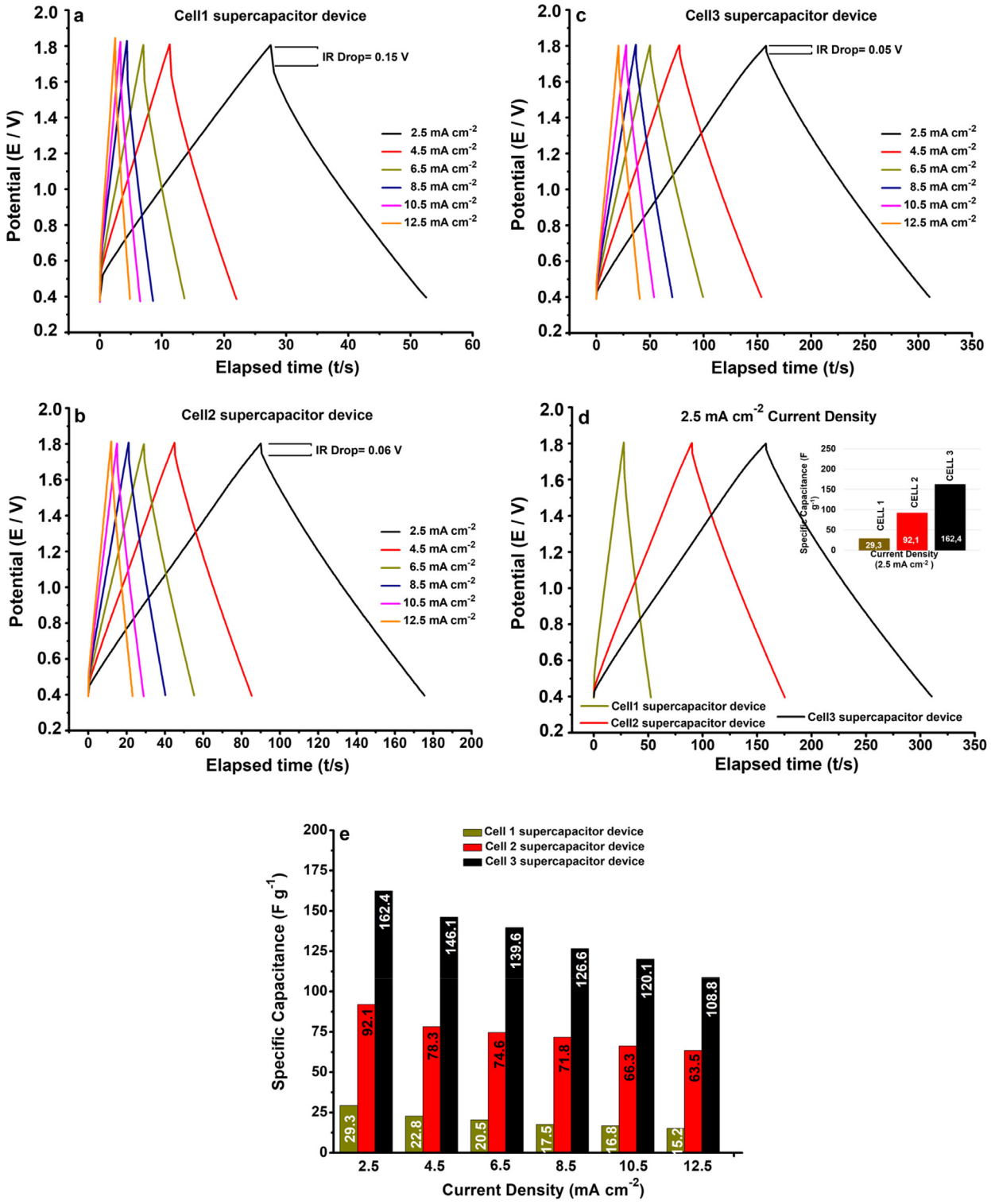


**Fig. 7.** GCD plots of (a) **Cell1**, (b) **Cell2** and (c) **Cell3** solid-state flexible supercapacitor devices at different current densities from 2.5 to 12.5 mA $cm^{-2}$, (d) comparative GCD curves of supercapacitor devices at 2.5 mA $cm^{-2}$ current density and (e) specific capacitance changes of **Cell1, Cell2** and **Cell3** as a function of current density.

Cell 3 (from 162.4 to 108.8 F $g^{-1}$), respectively, as seen in Fig. 7e. The relatively lower rate capability performances in the case of supercapacitor device configurations compared to three-electrode cell measurements resulted from the difficulties in ion movement and penetration in polymeric gel electrolyte media, as an expected behavior.

The long-term cycle life and high mechanical stability are considered as essential requirements for practical supercapacitor applications, as well as charge storage performance parameters (specific capacitance, energy and power densities). An effecient flexible supercapacitor device should exhibit the features of excellent flexibility and very long operation life without a remarkable loss of specific capacitance. Our flexible solid-state supercapaci-

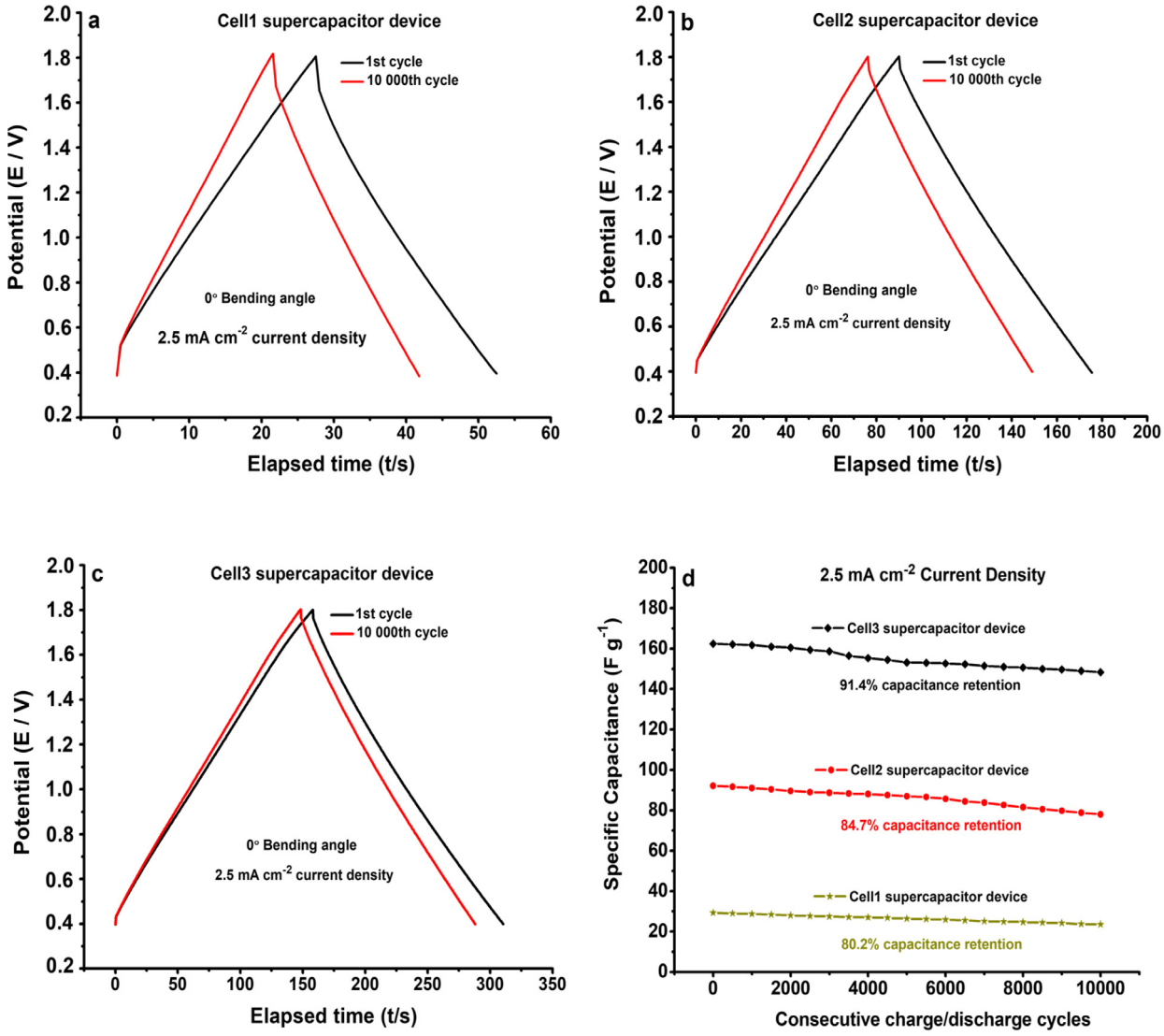


**Fig. 8.** Long-term cycling stabilities of (a) **Cell1**, (b) **Cell2**, (c) **Cell3** solid-state flexible supercapacitor devices at 2.5 mA $cm^{-2}$ current density under 0° bending angle for 10,000 charge/discharge cycles and (d) specific capacitance retentions of supercapacitor devices over 10,000 charge/discharge cycles at 2.5 mA $cm^{-2}$ current density.

tor devices were initially subjected to 10 000 consecutive galvanic charge/discharge cycles at 2.5 mA $cm^{-2}$ constant current density from 0.4 to 1.8 V in order to evaluate their long-term cycle lifes and the change in charge storage capacities. At the end of 10 000 cycles, Cell 1, Cell 2 and Cell 3 reached capacitance retention rates of 80.2% (from 29.3 to 23.5 F $g^{-1}$), 84.7% (from 92.1 to 78 F $g^{-1}$) and 91.4% (from 162.4 to 148.4 F $g^{-1}$), respectively, as presented in **Fig. 8a–d**.

These acceptable reductions in specific capacitances of flexible solid-state supercapacitors confirm that the polymeric networks of PSEDEN1, PSEDEN2 and PSEDEN3 could tolerate structural deformation caused by volumetric changes (shrinking and swelling) on the polymer backbones during repetitive charge/discharge processes. Similarly, mechanical stability tests of flexible solid-state supercapacitor devices were performed with a typically GCD technique at a current density of 2.5 mA $cm^{-2}$ in the same potential range under different bending angles (0°, 45°, 90°, 135° and 170°). **Fig. 9a–d** clearly indicate that Cell 1, Cell 2 and Cell 3 still maintained a large amount of their initial specific capacitance when they were bent from 0° to 170° The device gravimetric capacitance performances of Cell 1, Cell 2 and Cell 3 only decreased by 3.4%, 4.66% and 1.97%, respectively, even at extreme bending conditions (bending angle of 170°). These results confirm that our novel redox-active electrode materials have desirable mechanical features which can meet the fundamental requirements for the potential applications of high-performance energy storage devices in flexible electronic technology.

The electronic and kinetic properties of flexible solid-state supercapacitor devices were tested using EIS. As seen in corresponding Nyquist plots (**Fig. 10a–d**), Cell 1, Cell 2 and Cell 3 exhibited a semicircle pattern in the high frequency region and a linear portion in the low frequency region, as expected of an ideal supercapacitor. Semicircle parts of Nyquist plots revealed that Cell 1, Cell 2 and Cell 3 not only have low equivalent series resistance (ESR), but also possess small charge transfer resistance ($R_{CT}$) (**Fig. 10a–c**). The ESR values were calculated to be 7.77 Ω for Cell 1, 5.34 Ω for Cell 2 and 3.29 Ω for Cell 3 while $R_{CT}$ values of Cell 1, Cell 2 and Cell 3 were measured as 15.03, 10.64 and 7.38 Ω.

The straight portions of Nyquist plots in the middle and low frequency region, known as Warburg impedance (W), gave important data about ion diffusion kinetics on flexible solid-state supercapacitor devices during charge storage process. **Fig. 10d** clearly indicates that Cell 3 drew a steeper and shorter Warburg curve along the imaginary part of its Nyquist plot than those of Cell 1 and

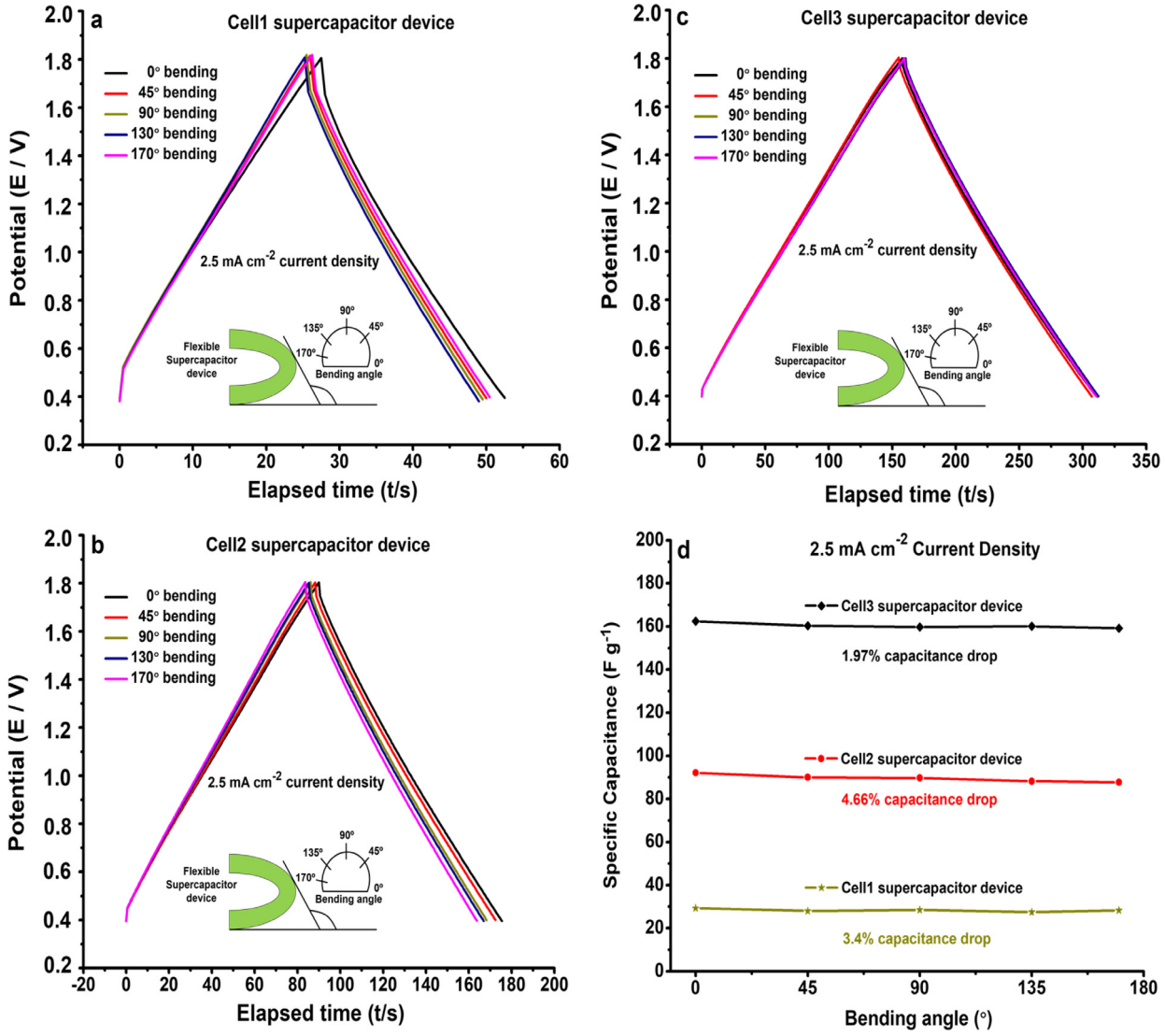


**Fig. 9.** Typical GCD curves of (a) **Cell1**, (b) **Cell2**, (c) **Cell3** solid-state flexible supercapacitor devices at 2.5 mA $cm^{-2}$ current density under various bending angle from 0 to 170° and (d) mechanical stability performance of supercapacitor devices as a function of bending angle at 2.5 mA $cm^{-2}$ current density.

Cell 2. This impedance characteristic means that a capacitive electrochemical double-layer on the surface of PSEDEN3 redox-active film formed faster compared to PSEDEN1 and PSEDEN2. Such obvious difference between ion diffusion kinetics of PSEDEN1, PSEDEN2 and PSEDEN3 redox-active electrode materials explains why Cell 3 has better capacitive performance. In this context, it is apparent that the results of EIS analysis are consistent with experimental data obtained from CV and GCD techniques.

## 4. Conclusion

In summary, we have presented a simple and effective strategy to diversify the morphological features of polymeric redox-active networks and consequently to enhance the electrochemical charge storage capacities of electrode materials. For this purpose, novel poly(terthiophene) derivatives containing oxyethylene substituents, PSEDEN1, PSEDEN2 and PSEDEN3, have been electrochemically prepared on the flexible mesh stainless steel current collector substrates and their capacitive performances have been evaluated following a standard test procedure (CV, GCD and EIS techniques). The effect of prolongation of oxyethylene chains on the morphological characteristics of PSEDEN1, PSEDEN2 and PSEDEN3 conducting polymer films was revealed by SEM observation in detail. Polymeric redox-active layers exhibited more appropriate 3D-dimensional network structures for easier and rapid ion diffusions or mobilities with increase in the oxyethylene chain length as a pendant group of the poly(terthiophene) backbones. In three-electrode test configuration, PSEDEN1, PSEDEN2 and PSEDEN3-based redox-active electrode materials reached up to 135 F $g^{-1}$, 212.8 F $g^{-1}$ and 403.3 F $g^{-1}$ gravimetric capacitance values, respectively, at a constant current density of 2.5 mA $cm^{-2}$ in the potential range of 0.4–1.8 V with low IR drop and good rate capacility performances. These differences in charge storage performances obtained for redox-active materials were correlated to the morphological properties of PSEDEN1, PSEDEN2 and PSEDEN3 polymeric films based on the evaluation of SEM images. Furthermore, symmetrical flexible solid-state supercapacitor devices with polymer gel electrolyte were also assembled using PSEDEN1, PSEDEN2 and PSEDEN3 redox-active electrode materials. These assembled device (Cell 1, Cell 2 and Cell 3) delivered competitive specific capacitances ($C_{spec}$= 162.4 F $g^{-1}$, 92.1 F $g^{-1}$ and 29.3 F $g^{-1}$), energy densities (SE= 41.1 W h $kg^{-1}$, 22.9 W h $kg^{-1}$ and 6.35 W h $kg^{-1}$) and power densities (SP= 986.4 W $kg^{-1}$, 937.7 W $kg^{-1}$ and 929 W $kg^{-1}$) in two-electrode setup. Notably, flexible super-

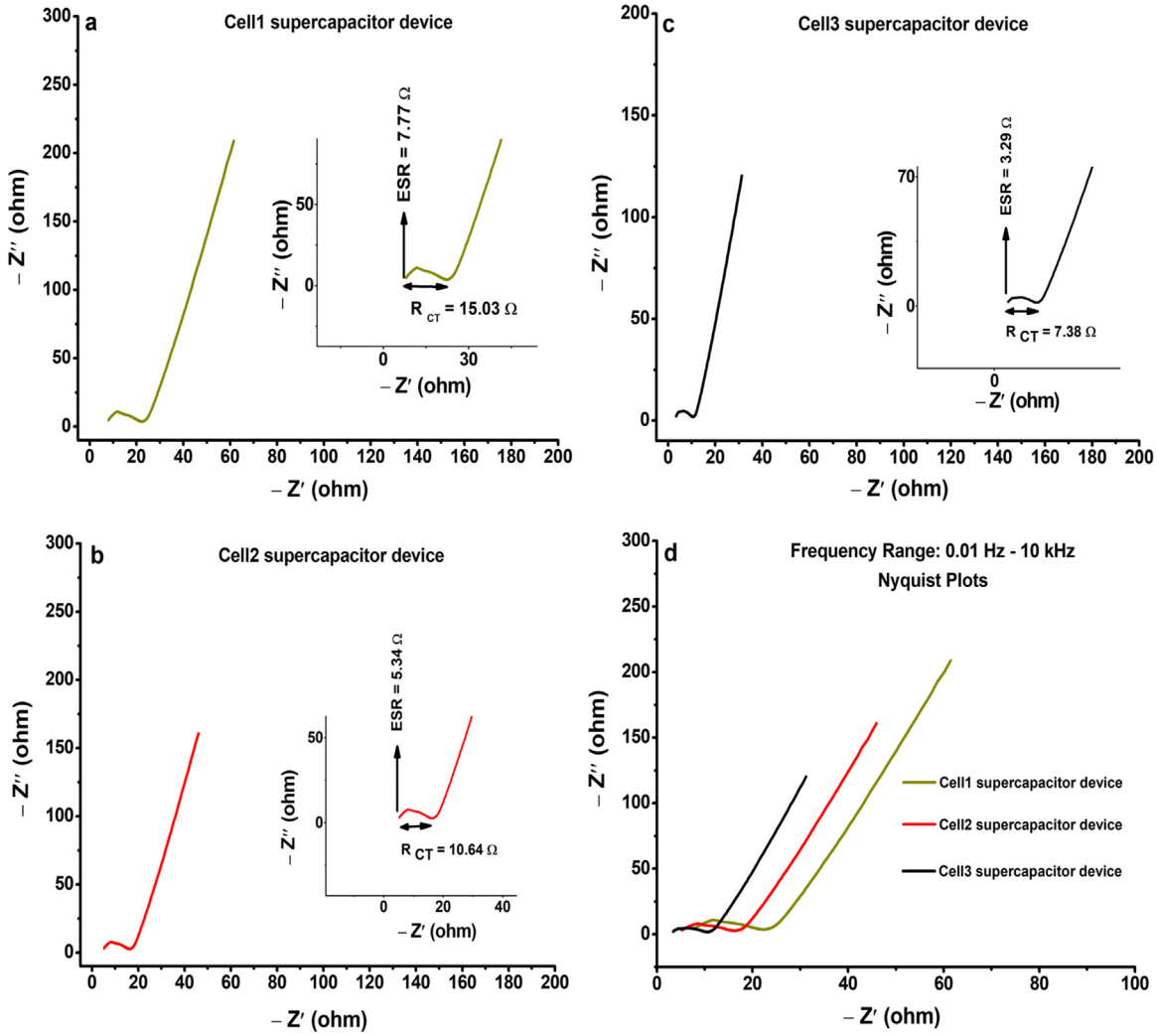


**Fig. 10.** Nyquist plots of (a) **Cell1**, (b) **Cell2**, (c) **Cell3** solid-state flexible supercapacitor devices and (d) comparative Nyquist impedance plots of supercapacitor devices in the frequency range of 10,000 to 0.01 Hz at 0.0 V DC applied voltage.

capacitor devices exhibited not only high long-term cycle life performances with good capacitance retentions (close to 92%) over 10 000 consecutive galvanic charge/discharge cycles, but also excellent mechanical stabilities (1.97% capacitance loss) under various bending conditions at 2.5 mA $cm^{-2}$ constant current density from 0.4 to 1.8 V. All results endorse that different charge storage capacities could be obtained with conducting polymer derivatives having similar chemical structures only depending on the morphological diversity. In this context, it is concluded that molecular design approach can be effectively used to influence morphological characteristics and enhance capacitive performance of electroactive materials in various conducting polymer-based charge storage applications.

## Declaration of Competing Interest

The authors declare that they have no known competing financial interests or personal relationships that could have appeared to influence the work reported in this paper.

## Credit authorship contribution statement

**Deniz Yiğit:** Conceptualization, Formal analysis, Methodology, Validation, Investigation, Writing – original draft. **Mustafa Güllü:** Supervision, Project administration, Writing – review & editing.

## Acknowledgments

This research was supported by the Scientific and Technological Research Council of Turkey (TÜBİTAK, Grant No: KBAG-114Z167). We gratefully thank TÜBİTAK (KBAG-114Z167) for its generously financial support.

## Supplementary materials

Supplementary data associated with this article can be found, in the online version, at 10.1016/j.electacta.2021.138662.

## References

[1] C. Tao, L. Dai, Flexible supercapacitors based on carbon nanomaterials, J. Mater. Chem. A 2 (2014) 10756–10775.
[2] L. Dang, C. Xu, Y. Li, Z. Hang, F. Kang, Q. Yang, X. Zhao, Flexible electrodes and supercapacitors for wearable energy storage: a review by category, J. Mater. Chem. A 4 (2016) 4659–4685.
[3] X. Zhang, Z. Lin, B. Chen, S. Sharma, C. Wong, W. Zhang, Y. Deng, Solid-state, flexible, high strength paper-based supercapacitors, J. Mater. Chem. A 1 (2013) 5835–5839.
[4] M.S. Halper, J.C. Ellenbogen, in: Supercapacitors: A Brief Overview, The MITRE Corporation, McLean, Virginia, USA, 2006, pp. 1–34.
[5] K.H. An, W.S. Kim, Y.S. Park, Y.C. Chai, S.M. Lee, D.C. Chung, D.J. Bae, S.C. Lim, Y.H. Lee, Supercapacitors using single-walled carbon nanotube electrodes, Adv. Mater. 13 (2001) 497–500.

[6] Q. Jiang, M.Z. Qu, G.M. Zhou, B.L. Zhang, Z.L. Yu, A study of activated carbon nanotubes as electrochemical super capacitors electrode materials, Mater. Lett. 57 (2002) 988–991.
[7] D.W. Lawrence, C. Tran, A.T. Mallajoysula, S.K. Doorn, A. Mohite, G. Gupta, V. Kalra, High-energy density nanofiber-based solid-state supercapacitors, J. Mater. Chem. A 4 (2016) 160–166.
[8] B.H. Kim, K.S. Yang, J.P. Ferraris, Highly conductive, mesoporous carbon nanofiber web as electrode material for high-performance supercapacitors, Electrochim. Acta 75 (2012) 325–331.
[9] C. Liu, Z. Yu, D. Neff, A. Zhamu, B.Z. Jang, Graphene-based supercapacitor with an ultrahigh energy density, Nano Lett. 10 (2010) 4863–4886.
[10] T.Y. Kim, G. Jung, S. Yoo, K.S. Suh, R.S. Ruoff, Activated graphene-based carbons as supercapacitor electrodes with macro- and mesopores, ACS Nano 7 (2013) 6899–6905.
[11] D.W. Park, N.A. Canas, M. Schwan, B. Milow, L. Ratke, K.A. Friedrich, A dual mesopore C-aerogel electrode for a high energy density supercapacitor, Curr. Appl. Phys. 16 (2016) 658–664.
[12] Y. Xu, B. Ren, S. Wang, L. Zhang, Z. Liu, Carbon aerogel-based supercapacitors modified by hummers oxidation method, J. Colloid Interface Sci. 527 (2018) 25–32.
[13] Q. Li, H. Wang, Q. Dai, J. Yang, Y. Zhong, Novel activated carbons as electrode materials for electrochemical capacitors from a series of starch, Solid State Ion. 179 (2008) 269–273.
[14] E. Frackowiaka, F. Beǵuin, Carbon materials for the electrochemical storage of energy in capacitors, Carbon 39 (2001) 937–950 N Y.
[15] B. Park, C.D. Lokhande, H. Park, K. Jung, O. Joo, Electrodeposited ruthenium oxide ($RuO_2$) films for electrochemical supercapacitors, J. Mater. Sci. 39 (2004) 4313–4317.
[16] Y. Liu, F. Zhou, V. Ozolins, Ab Initio Study of the Charge-Storage Mechanisms in $RuO_2$-Based Electrochemical Ultracapacitors, J. Phys. Chem. C 116 (2012) 1450–1457.
[17] H. Xia, Y.S. Meng, G. Yuan, C. Cui, Luc L, A symmetric $RuO_2/RuO_2$ Supercapacitor operating at 1.6V by using a neutral aqueous electrolyte, Electrochem. Solid State Lett. 15 (2012) A60–A63.
[18] B. Saravanakumar, K.K. Purushothaman, G. Muralidharan, Interconnected $V_2O_5$ nanoporous network for high-performance supercapacitors, ACS Appl. Mater. Interfaces 4 (2012) 4484–4490.
[19] J. Yanga, T. Lana, J. Liub, Y. Songa, M. Weia, Supercapacitor electrode of hollow spherical $V_2O_5$ with a high pseudocapacitance in aqueous solution, Electrochim. Acta 105 (2013) 489–495.
[20] N. Wang, Y. Zhang, T. Hu, Y. Zhao, C. Meng, Facile hydrothermal synthesis of ultrahigh-aspect-ratio $V_2O_5$ nanowires for high-performance supercapacitors, Curr. Appl. Phys. 15 (2015) 493–498.
[21] X. Li, G. Wang, X. Wang, X. Li, J. Ji, Flexible supercapacitor based on $MnO_2$ nanoparticles via electrospinning, J. Mater. Chem. A 1 (2013) 10103–10106.
[22] A.G. Bosca, D. Belanger, Electrochemical characterization of $MnO_2$-based composite in the presence of salt-in-water and water-in-salt electrolytes as electrode for electrochemical capacitors, J. Power Sources 326 (2016) 9595–9603.
[23] N. Kaabia, B. Choucheneb, V. Mabroukc, F. Matoussid, E.S.B.H. Hmidaa, Electrochemical properties of a modified electrode with $\delta$-$MnO_2$-based new nanocomposites, Solid State Ion. 325 (2018) 74–79.
[24] Y. Liu, Y. Jiao, Z. Zhang, F. Qu, A. Umar, X. Wu, Hierarchical $SnO_2$ nanostructures made of intermingled ultrathin nanosheets for environmental remediation, smart gas sensor, and supercapacitor applications, ACS Appl. Mater. Interfaces 6 (2014) 2174–2184.
[25] Y.J. Hong, J. Yoon, J. Lee, Y.C. Kang, A new concept for obtaining $SnO_2$ fiber-in–tube nanostructures with superior electrochemical properties, Chem. Eur. J. 21 (2015) 371–376.
[26] Q. Zhao, L. Ma, Q. Zhang, C. Wang, X. Xu, $SnO_2$-based nanomaterials: synthesis and application in lithium-ion batteries and supercapacitors, J. Nanomater. (2015) 1–15.
[27] C. Yuan, X. Zhang, L. Su, B. Gao, L. Shen, Facile synthesis and self-assembly of hierarchical porous NiO nano/micro spherical superstructures for high performance supercapacitors, J. Mater. Chem. 19 (2009) 5772–5777.
[28] M. Khairya, S.A. El-Safty, Mesoporous NiO nanoarchitectures for electrochemical energy storage: influence of size, porosity, and morphology, RSC Adv. 3 (2013) 23801–23809.
[29] G. Cheng, Y. Yanb, R. Chen, From Ni-based nanoprecursors to NiO nanostructures: morphology-controlled synthesis and structure-dependent electrochemical behavior, New J. Chem. 39 (2015) 676–682.
[30] X. Lu, G. Wang, T. Zhai, M. Yu, J. Gan, Y. Tong, Y. Li, Hydrogenated $TiO_2$ nanotube arrays for supercapacitors, Nano Lett. 12 (2012) 1690–1696.
[31] X. He, C.P. Yang, G.L. Zhanga, D.W. Shi, Q.A. Huang, H.B. Xiao, Y. Liu, R. Xiong, Supercapacitor of $TiO_2$ nanofibers by electrospinning and KOH treatment, Mater. Des. 106 (2016) 74–80.
[32] S.S. Raut, G.P. Patil, P.C. Chavan, P.R. Sankapal, Vertically aligned $TiO_2$ nanotubes: highly stable electrochemical supercapacitor, J. Electroanal. Chem. 780 (2016) 197–200.
[33] G.A. Snook, P. Kao, A.S. Best, Conducting-polymer-based supercapacitor devices and electrodes, J. Power Sources 196 (2011) 1.
[34] C. Arbizzani, M.C. Gallazzi, M. Mastragostino, M. Rossi, F. Soavi, Capacitance and cycling stability of poly (alkoxythiophene) derivative electrodes, Electrochem. Commun. 3 (2001) 16–19.
[35] P. Soudan, P. Lucas, H.A. Ho, D. Jobin, L. Breau, D. Bélanger, Synthesis, chemical polymerization and electrochemical properties of low band gap conducting polymers for use in supercapacitors, J. Mater. Chem. 11 (2001) 773–782.
[36] K.R. Prasad, M. Munichandraiah, Fabrication and evaluation of 450 F electrochemical redox supercapacitors using inexpensive and high performance, polyaniline coated, stainless-steel electrodes, J. Power Sources 112 (2002) 443–451.
[37] F. Marchioni, J. Yang, W. Walker, F. Wudl, A low band gap conjugated polymer for supercapacitor devices, J. Phys. Chem. B 110 (2006) 22202–22206.
[38] M.M. Khandpekar, R.K. Kushwaka, S.P. Pati, Design, fabrication and evaluation of 5F-5V prototype of solid-sate PANI based supercapacitors, Solid State Electron. 62 (2011) 156–160.
[39] C. Arbizzani, M. Mastragostino, L. Meneghello, Polymer-based redox supercapacitors: a comparative study, Electrochim. Acta 41 (1996) 21–26.
[40] C. Arbizzania, M. Mastragostino, F. Soavi, New trends in electrochemical supercapacitors, J. Power Sources 100 (2001) 164–170.
[41] K.R. Prasad, N. Miura, Electrochemical synthesis and characterization of nanostructured tin oxide for electrochemical redox supercapacitors, Electrochem. Commun. 6 (2004) 849–852.
[42] L.Z. Fan, J. Maier, High-performance polypyrrole electrode materials for redox supercapacitors, Electrochem. Commun. 8 (2006) 937–940.
[43] V. Gupta, N. Miura, High performance electrochemical supercapacitor from electrochemically synthesized nanostructured polyaniline, Mater. Lett. 60 (2006) 1466–1469.
[44] V. Gupta, N. Miura, Electrochemically deposited polyaniline nanowire's network: a high- performance electrode material for redox supercapacitor, Electrochem. Solid State Lett. 8 (2005) A630.
[45] K. Wang, J. Huang, Z. Wei, Conducting polyaniline nanowire arrays for high performance supercapacitors, J. Phys. Chem. C 114 (2010) 8062–8067.
[46] Y.H. Kim, J. Hwang, J.I. Son, Y.B. Shim, Synthesis, electrochemical, and spectroelectrochemical properties of conductive poly-[2,5-*di*-(2-*thienyl*)-1H-*pyrrole*-1-(*p*-*benzoic acid*)], Synth. Met. 160 (2010) 413–418.
[47] P. Sivaramana, R.K. Kushwahaa, K. Shashidharaa, V.R. Handea, A.P. Thakura, A.B. Samuia, M.M. Khandpekar, All solid supercapacitor based on polyaniline and crosslinked sulfonated poly[*ether ether ketone*], Electrochim. Acta 55 (2010) 2451–2456.
[48] D.S. Dhawalea, A. Vinub, C.D. Lokhandea, Stable nanostructured polyaniline electrode for supercapacitor application, Electrochim. Acta 56 (2011) 9482–9487.
[49] M. Liu, Y. Miao, C. Zhang, W.W. Tjiu, Z. Yang, H. Penga, T. Liu, Hierarchical composites of polyaniline–grapheme nanoribbons–carbon nanotubes as electrode materials in all-solid-state supercapacitors, Nanoscale 5 (2013) 7312–7320.
[50] N.H. Khdary, M.E. Abdesalam, G.E. Enany, Mesoporous polyaniline films for high performance supercapacitors, J. Electrochem. Soc. 161 (2014) G63–G68.
[51] A. Eftekhari, L. Li, Y. Yang, Polyaniline supercapacitors, J. Power Sources 347 (2017) 86–107.
[52] B.C. Kim, J.M. Ko, G.G. Wallace, A novel capacitor material based on Nafion–doped polypyrrole, J. Power Sources 177 (2008) 665–668.
[53] J. Wang, Y. Xu, J. Wang, Du X, Toward a high specific power and high stability polypyrrole supercapacitors, Synth. Met. 161 (2011) 1141–1144.
[54] S. Biswas, L.T. Drzal, Multilayered nanoarchitecture of graphene nanosheets and polypyrrole nanowires for high performance supercapacitor electrodes, Chem. Mater. 22 (2010) 5667–5671.
[55] Y. Song, T. Liu, X. Xu, D. Feng, Y. Li, X. Liu, Pushing the cycling stability limit of polypyrrole for supercapacitors, Adv. Funct. Mater. 25 (2015) 4626–4632.
[56] Q. Yang, Z. Hou, T. Huang, Self-assembled polypyrrole film by interfacial polymerization for supercapacitor applications, J. Appl. Polym. Sci. 132 (11) (2015) 41615.
[57] G. Chen, Z. Liu, J. Lin, N. Li, Y. Su, Hierarchical polypyrrole based composites for high performance asymmetric supercapacitors, J. Power Sources 283 (2015) 484–493.
[58] J. Xu, D. Wang, L. Fan, Y. Yuan, W. Wei, R. Liu, S. Gu, W. Xu, Fabric electrodes coated with polypyrrole nanorods for flexible supercapacitor application prepared via a reactive self-degraded template, Org. Electron. 26 (2015) 292–299.
[59] I. Shown, A. Ganguly, L. Chen, K. Chen, Conducting polymer-based flexible supercapacitor, Energy Sci. Eng. 3 (2015) 2–26.
[60] A. Laforgue, P. Simon, C. Sarrazin, J. Fauvarque, Polythiophene-based supercapacitors, J. Power Sources 80 (1999) 142–148.
[61] E. Hür, G.A. Varol, A. Arslan, The study of polythiophene, poly(3-methylthiophene) and poly(3,4-ethylenedioxythiophene) on pencil graphite electrodeas an electrode active material for supercapacitor applications, Synth. Met. 184 (2013) 16–22.
[62] J.P. Ferraris, M.M. Eissa, I.D. Brotherston, D.C. Loveaday, Performance evaluation of poly(3-Phenylthiophene) derivatives as active materials for electrochemical capacitor applications, Chem. Mater. 10 (1998) 3528–3535.
[63] M. Mastragostino, C. Arbizzani, F. Soavi, Conducting polymers as electrode materials in supercapacitors, Solid State Ion. 148 (2002) 493–498.
[64] D.Y. Liu, J.R. Reynolds, Dioxythiophene based polymer electrodes for supercapacitor module, ACS Appl. Mater. Interfaces 2 (2010) 3586–3593.
[65] E. Ermiş, D. Yiğit, M. Güllü, Synthesis of poly (N-alkly-3,4-dihydrothieno [3,4-b][1,4]oxazine) derivatives and investigation of their supercapacitive performances for charge storage, Electrochim. Acta 90 (2013) 623–633.
[66] K.S. Ryu, Y.G. Lee, Y.S. Hang, Y.J. Park, X. Wu, M.K. Kim, M.G. Kang, N.G. Park, S.H. Chang, Poly(ethylenedioxythiopene) (PEDOT) as polymer electrode in redox supercapacitor, Electrochim. Acta 50 (2004) 843–847.
[67] J.H. Huang, C.W. Chu, Achieving efficient poly(3,4-ethylenedioxythiophene)-based supercapacitors by controlling the polymerization, Electrochim. Acta 56 (2011) 7228–7234.

[68] V. Armel, J. Rivnay, G. Malliaras, B.W. Jansen, Unexpected interaction between PEDOT and phosphonium ionics liquids, J. Am. Soc. 135 (2013) 11309–11313.
[69] D. Yiğit, M. Güllü, N-substituted poly(3,6-dithienylcarbazole) derivatives: a new class of redox-active electrode materials for high-performance flexible solid-state pseudocapacitors, J. Mater. Chem. A 5 (2017) 609–618.
[70] A.M. Bryan, L.M. Santino, Y. Lu, S. Acharya, J.M. D'Arcy, Conducting polymers for pseudocapacitive energy storage, Chem. Mater. 28 (2016) 5989–5998.
[71] Q. Meng, K. Cai, Y. Chen, L. Chen, Research progress on conducting polymer based supercapacitor electrode materials, Nano Energy 36 (2017) 268–285.
[72] S. Cosnier, A. Karyakin, Electropolymerization: Concepts, Materials and Applications, John Wiley & Sons, 2011.
[73] K. Cysewska, J. Karczewski, P. Jasiński, Influence of electropolymerization conditions on the morphological and electrical properties of PEDOT film, Electrochim. Acta 176 (2015) 156–161.
[74] D. Yigit, M. Aykan, M. Gullu, Substituent effect on supercapacitive performances of conducting polymer-based redox electrodes: poly (3,4-bis (alkyloxy) 2,2: 5,2-terthiophene) derivatives, J. Polym. Sci. Part A Polym. Chem. 56 (2018) 480–495.
[75] D. Yiğit, M. Güllü, Capacitive properties of novel N-alkyl substituted poly (3, 6-dithienyl-9H carbazole)s as redox electrode materials and their symmetric micro-supercapacitor applications, Electrochim. Acta 282 (2018) 64–80.
[76] P.M. Beaujuge, J. Subbiah, K.R. Choudhury, S. Ellinger, T.D. McCarley, F. So, J.R. Reynolds, Green dioxythiophene-benzothiadiazole donor- acceptor copolymers for photovoltaic device applications, Chem. Mater. 22 (2010) 2093–2106.
[77] J. Roncali, R. Garreau, A. Yassar, P. Marque, F. Garnier, M. Lemaire, Effects of steric factors on the electrosynthesis and properties of conducting poly (3-alkylthiophenes), J. Phys. Chem. 91 (1987) 6706–6714.
[78] J. Roncali, A. Gorgues, M. Jubault, Effects of substitution of the median thiophene ring on the electrodeposition and structure of poly (terthienyls), Chem. Mater. 5 (1993) 1456–1464.
[79] I. Namal, A.C. Ozelcaglayan, Y.A. Udum, L. Toppare, Synthesis and electrochemical characterization of fluorene and benzimidazole containing novel conjugated polymers: effect of alkyl chain length on electrochemical properties, Eur. Polym. J. 49 (2013) 3181–3187.
[80] D. Mo, S. Zhen, J. Xu, W. Zhou, B. Lu, G. Zhang, G.Z. Zhipeng, W.S. Zhang, Z. Feng, Alkyl chain engineering in the hybrid bithiophene-3, 4-ethylenedioxythiophene: synthesis, electronic properties, and electropolymerization, Synth. Met. 198 (2014) 19–30.
[81] Y. Sun, X. Zhao, G. Zhu, M. Li, X. Zhang, H. Yang, B. Lin, Twisted ladder-like donor-acceptor polymers as electrode materials for flexible electrochromic supercapacitors, Electrochim. Acta 333 (2020) 135495.
[82] W.D. Oosterbaan, J.C. Bolsée, A. Gadisa, V. Vrindts, S. Bertho, J. D'Haen, T.J. Cleij, L. Lutsen, C.R. McNeill, L. Thomsen, J.V. Manca, D. Vanderzande, Alkyl-chain-length-independent hole mobility via morphological control with poly (3-alkylthiophene) nanofibers, Adv. Funct. Mater. 20 (2010) 792–802.
[83] A. Hamidi-Sakr, L. Biniek, J.L. Bantignies, D. Maurin, L. Herrmann, N. Leclerc, P. Lévêque, V. Vijayakumar, N. Zimmermann, M. Brinkmann, A versatile method to fabricate highly in-plane aligned conducting polymer films with anisotropic charge transport and thermoelectric properties: the key role of alkyl side chain layers on the doping mechanism, Adv. Funct. Mater. 27 (2017) 1700173.
[84] X. Liu, B. He, A. Garzón-Ruiz, A. Navarro, T.L. Chen, M.A. Kolaczkowski, F. Shizhen, L. Zhang, A.A. Christopher, C. Junwu Chen, Y. Liu, Unraveling the main chain and side chain effects on thin film morphology and charge transport in quinoidal conjugated polymers, Adv. Funct. Mater. 28 (2018) 1801874.
[85] C.G. Wu, Y.C. Lin, M.J. Chan, L.N. Chien, Steric effect and mobility of the alkyl chain in regio-irregular poly-3-alkylthiophenes, J. Polym. Sci. Part B Polym. Phys. 37 (1999) 1763–1772.
[86] C. Duan, R.E. Willems, J.J. van Franeker, B.J. Bruijnaers, M.M. Wienk, R.A. Janssen, Effect of side chain length on the charge transport, morphology, and photovoltaic performance of conjugated polymers in bulk heterojunction solar cells, J. Mater. Chem. A 4 (2016) 1855–1866.
[87] X. Bai, X. Hu, S. Zhou, Flexible supercapacitors based on 3D conductive network electrodes of poly (3,4-ethylenedioxythiophene)/non-woven fabric composites, RSC Adv. 5 (2015) 43941–43948.
[88] B.N. Reddy, M. Deepa, A.G. Joshi, Highly conductive poly (3,4-ethylenedioxypyrrole) and poly (3,4-ethylenedioxythiophene) enwrapped $Sb_2S_3$ nanorods for flexible supercapacitors, Phys. Chem. Chem. Phys. 16 (2014) 2062–2071.
[89] H. Zhang, L. Hu, J. Tu, S. Jiao, Electrochemically assembling of polythiophene film in ionic liquids (ILs) microemulsions and its application in an electrochemical capacitor, Electrochim. Acta 120 (2014) 122.
[90] S. Patra, N. Munichandraiah, Supercapacitor studies of electrochemically deposited PEDOT on stainless steel substrate, J. Appl. Polym. Sci. 106 (2007) 1160.
[91] D. Moa, W. Zhoua, X. Maa, J. Xua, D. Zhua, B. Lu, Electrochemical synthesis and capacitance properties of a novel poly(3,4-ethylenedioxythiophene bissubstituted bithiophene)electrode material, Electrochim. Acta 132 (2014) 67.
[92] J.G. Ibanez, M.E. Rincón, S. Gutierrez-Granados, M. Chahma, O.A. Jaramillo-Quintero, B.A. Frontana-Uribe, Conducting polymers in the fields of energy, environmental remediation and chemical–chiral sensors, Chem. Rev. 118 (2018) 4731–4816.